

RESEARCH

Open Access



PD-L1 and IFN- γ modulate Non-Small Cell Lung Cancer (NSCLC) cell plasticity associated to immune checkpoint inhibitor (ICI)-mediated hyperprogressive disease (HPD)

Stefania Angelicola^{1,2}, Francesca Giunchi³, Francesca Ruzzi², Mariateresa Frascino⁴, Mary Pitzalis⁴, Laura Scalambra², Maria Sofia Semprini², Olga Maria Pittino², Chiara Cappello², Irene Siracusa⁴, Ilaria Candida Chillico⁴, Martina Di Noia⁴, Cristian Turato⁴, Silvia De Siervi⁴, Francesco Lescai⁵, Teresa Ciavattini⁶, Giulia Lopatriello⁶, Luca Bertoli⁶, Hugo De Jonge⁴, Luisa Iamele⁴, Annalisa Altimari⁷, Elisa Gruppioni⁷, Andrea Ardizzoni^{1,8}, Marzia Rossato^{6,9}, Francesco Gelsomino^{1*†}, Pier-Luigi Lollini^{2,10†} and Arianna Palladini^{4,11*†} 

Abstract

Background Non-Small Cell Lung Cancer (NSCLC) is the leading cause of cancer death worldwide. Although immune checkpoint inhibitors (ICIs) have shown remarkable clinical efficacy, they can also induce a paradoxical cancer acceleration, known as hyperprogressive disease (HPD), whose causative mechanisms are still unclear.

Methods This study investigated the mechanisms of ICI resistance in an HPD-NSCLC model. Two primary cell cultures were established from samples of a NSCLC patient, before ICI initiation ("baseline", NSCLC-B) and during HPD ("hyperprogression", NSCLC-H). The cell lines were phenotypically and molecularly characterized through immunofluorescence, Western Blotting and RNA-Seq analysis. To assess cell plasticity and aggressiveness, cellular growth patterns were evaluated both in vitro and in vivo through 2D and 3D cell growth assays and patient-derived xenografts establishment. In vitro investigations, including the evaluation of cell sensitivity to interferon-gamma (IFN- γ) and cell response to PD-L1 modulation, were conducted to explore the influence of these factors on cell plasticity regulation.

Results NSCLC-H exhibited increased expression of specific CD44 isoforms and a more aggressive phenotype, including organoid formation ability, compared to NSCLC-B. Plastic changes in NSCLC-H were well described by a deep transcriptome shift, that also affected IFN- γ -related genes, including PD-L1. IFN- γ -mediated cell growth inhibition was compromised in both 2D-cultured NSCLC-B and NSCLC-H cells. Further, the cytokine induced a partial activation of both type I and type II IFN-pathway mediators, together with a striking increase in NSCLC-B growth in 3D cell

[†]Francesco Gelsomino, Pier-Luigi Lollini and Arianna Palladini contributed equally to this work.

*Correspondence:

Francesco Gelsomino
francesco_gelsomino@aosp.bo.it
Arianna Palladini
arianna.palladini@unipv.it

Full list of author information is available at the end of the article



culture systems. Finally, low IFN- γ doses and PD-L1 modulation both promoted plastic changes in NSCLC-B, increasing CD44 expression and its ability to produce spheres.

Conclusions Our findings identified plasticity as a relevant hallmark of ICI-mediated HPD by demonstrating that ICIs can modulate the IFN- γ and PD-L1 pathways, driving tumor cell plasticity and fueling HPD development.

Keywords Non-Small Cell Lung Cancer, Immune checkpoint inhibitors, Tumor plasticity, Hyperprogressive disease, IFN- γ , PD-L1

Introduction

Lung cancer is the leading cause of cancer-related death worldwide [1]. Non-Small Cell Lung Cancer (NSCLC) represents the most common histological subtype, accounting for approximately 85% of all lung cancer diagnoses [1]. The presence of nonspecific clinical symptoms and the paucity of effective screening programs lead to delayed NSCLC diagnosis and reduced survival rates for these patients [1]. The clinical management of NSCLC appears even more difficult if we consider that only about one third of cases harbor a druggable driver alteration [2]. The approval in clinical practice of monoclonal antibodies targeting immune checkpoint molecules, including PD-1 (Programmed Cell Death Protein-1) and PD-L1 (Programmed Cell Death Ligand 1), able to restore anti-tumor immunity, led to a paradigm shift in the treatment of non-oncogene-addicted advanced NSCLC [3]. Immune checkpoint inhibitors (ICIs) have indeed demonstrated unprecedented durable responses and significant improvement in patients' survival in a variety of tumor types, becoming the standard of care for the treatment of several malignancies, including NSCLC [4]. Nevertheless, despite the impressive breakthrough provided by ICIs, only 20–30% of NSCLC patients derive a long-term survival benefit from these drugs due to the development of both primary and acquired resistance [5]. In addition, the success of ICI therapy is hindered by the development of atypical patterns of tumor response of which hyperprogressive disease (HPD) is the most controversial and detrimental one [6]. The phenomenon of hyperprogression was first assessed in retrospective studies involving patients affected by different tumor types, who showed a paradoxical acceleration of tumor growth, reduced survival and early fatality under ICI therapy [6, 7]. Evidence suggests an incidence rate of HPD in NSCLC ranging between 8 and 21% [7]. Even though several factors associated with hyperprogression have been pointed out [8–10], effective predictive biomarkers of HPD occurrence are not yet available and whether the mechanisms regulating this phenomenon are tumor-dependent or not has to be still clarified [7].

In this paper, we investigated the roles of interferon-gamma (IFN- γ) signaling pathway and PD-L1 modulation in the development of HPD in advanced NSCLC

undergoing ICI therapy. For this purpose, we established two NSCLC cell lines from tumor biopsies of an HPD patient, obtained before treatment initiation (NSCLC-B cell line) and at the time of evidence of hyperprogressive disease (NSCLC-H cell line). The two cell models showed deep phenotypic differences, evidencing how plasticity drove tumor evolution from NSCLC-B to the more aggressive NSCLC-H model. Additionally, we proved the involvement of IFN- γ and PD-L1 in the modulation of tumor plasticity, suggesting a possible, intriguing tumor-dependent mechanism of survival and “self-empowerment” in tumors of HPD patients undergoing ICI therapy.

Materials and methods

Clinical setting and human cell lines

A 64-year-old, former light smoker (10 pack/year) woman was diagnosed with stage IVA NSCLC. At the time of hyperprogression under pembrolizumab (Keytruda, Merck) treatment, the tumor was classified as a poorly differentiated, stage IVB NSCLC. Tumor samples were collected before and after treatment initiation, at three different time points. Two samples were obtained before treatment: one sample at the diagnosis (time of diagnosis, Tdx) and the other one a month after the diagnosis (time of baseline, Tb). The third sample was obtained three months after treatment initiation, at the time of radiological evidence of HPD (time of hyperprogression, Thy).

NSCLC-B cell line (B: “baseline”) was derived from the pleural effusion of the treatment-naïve patient at the Tb point, while NSCLC-H cell line (H: “hyperprogression”) was established from a subcutaneous thoracic tumor biopsy collected at the Thy point.

NSCLC-B primary cell culture was established after centrifugation of the pleural effusion of the patient, as previously described [11], while NSCLC-H primary cell culture was derived as follows: tumor biopsy was dissected with a sterile surgical scalpel. The obtained fragments were then placed into a 25 cm² PRIMARIA tissue culture flask (Corning Life Science, Tewksbury, MA, USA).

NSCLC-H2 and NSCLC-H3 cell lines were derived from tumor biopsies of two additional patients with stage IV NSCLC, who developed HPD after receiving immunotherapy or chemo-immunotherapy, respectively. The

cell lines were established following the same protocol used for the NSCLC-H cell line.

The two clinical cases in which we evaluated the expression of CD44 in tumor biopsies taken at baseline (T0) and at the time of the development of ICI resistance (T1), involve two patients with stage IV NSCLC who developed resistance to ICIs following chemo-immunotherapy.

All the cell lines were established and cultured in RPMI medium (Thermo Fisher Scientific, Monza, Italy) supplemented with 10% fetal bovine serum (FBS, Thermo Fisher Scientific), 100 U/mL penicillin and 10 µg/mL streptomycin (Thermo Fisher Scientific). Cells were cultured at 37°C in a humidified 5% CO₂ atmosphere and were split once or twice a week according to density.

Murine cell line

The BoLC.8M3 lung adenocarcinoma cell line was derived from the spontaneous lung tumor of a BALB/c transgenic mouse model in our laboratory. This transgenic model harbored the oncogenic KRAS^{G12D} mutation and a heterozygous knockout of the *p53* gene.

The cell line was established and cultured in DMEM medium (Thermo Fisher Scientific, Monza, Italy) supplemented with 20% FBS, 100 U/mL penicillin and 10 µg/mL streptomycin (Thermo Fisher Scientific). Cells were cultured at 37°C in a humidified 5% CO₂ atmosphere and were split once or twice a week according to density.

In vivo treatment with anti-PD-L1 monoclonal antibody

The experiments involving BoLC.8M3 cells were conducted in immunocompetent, 7–8-week-old male syngeneic BALB/c mice. The mice were randomized into an untreated group and a group treated with anti-PD-L1 antibody atezolizumab (Tecentriq, Genentech). BoLC.8M3 cells were subcutaneously (s.c.) injected at the dose of 10⁵ cells in a hind leg (n = 15 for each group). Starting from one day after cell injection, treated mice received intraperitoneal (i.p.) administrations of atezolizumab 10 mg/Kg bi-weekly, every 3 or 4 days, for the entire duration of the experiment. The control group received no treatment. Animals were checked weekly, and tumors were measured with calipers. Tumor volume was calculated as described previously and mice were sacrificed as described in the previous section.

All animal procedures were performed in accordance with European directive 2010/63/UE and Italian Law (No. DL26/2014). Experimental protocols were reviewed and approved by the institutional animal care and use committee of the University of Bologna and by the Italian Ministry of Health with letter 32/2020-PR.

Immunohistochemical and molecular analyses on tumor specimens

From formalin-fixed paraffin-embedded (FFPE) tumor blocks collected at different time points (Tdx, Tb and Thy), 3 µm-thick sections were cut. Hematoxylin and eosin (H&E) staining was performed on the FFPE sections and the immunohistochemistry studies were conducted with the automatic immunohistochemistry stainer of the instrument, Benchmark Ultra (Ventana/Roche Group Tucson, AZ, USA). The following pre-diluted antibodies were used: PD-L1 TPS (clone SP263, Ventana/Roche), TTF-1 (clone 8G7G3/1, Ventana/Roche) and Ber-EP4 (clone BER-EP4, Ventana/Roche). Immunostaining for CD44 was performed by using a polyclonal antibody (ab157107, AbCam plc, Cambridge, UK) at dilution 1:1200 and was conducted with antigen retrieval Cell Conditioning 1 for 40 min at 99°C. The revelation system used is OptiView DAB (12 min linker and 12 min HRP multimer) (Ventana/Roche).

The mutational profile of the sample obtained at the Tdx point was investigated by using the OncoPrint Focus Assay (Thermo Fisher Scientific), able to identify 35 hotspot genes, including *KRAS*. Sequencing was performed by using the Ion GeneStudio S5 (Thermo Fisher Scientific).

Whole transcriptome sequencing of NSCLC-B and NSCLC-H cell lines

Total RNA was extracted from three different in vitro passages (between 16th and 31st) of NSCLC-B and NSCLC-H two-dimensional (2D)-cultured cells using the GenUP Total RNA Kit (Biotechrabbit GmbH, Berlin, Germany), according to the manufacturer's instructions. RNA integrity was assessed by electrophoretic analysis on a 2100 Bioanalyzer (Agilent Technologies, Santa Clara, CA, USA) loaded with an RNA 6000 Nano Chip. All samples showed an RNA integrity number (RIN) > 8. RNA concentration was measured by a Qubit 4 fluorometer with a Qubit RNA BR Assay and RNA purity was assessed with a NanoDrop 8000 Spectrometer (Thermo Fisher Scientific). Total RNA libraries were prepared by IIGM–Italian Institute for Genomic Medicine (Turin, Italy) with the Illumina Stranded Total RNA Prep with Ribo-Zero Plus kit (Illumina Inc., San Diego, CA, USA), according to manufacturer's instructions without protocol modifications.

Quality of reads was assessed using the FastQC software [12]. STAR aligner (v2.7.9a) was used to identify differentially expressed isoforms, while gene and isoform expression quantification has been performed using RSEM (v1.3.1) [13] and Salmon (v0.13.1), respectively, based on the *Homo sapiens* Ensembl v.110 annotation.

Gene Ontology (GO) enrichment analysis of differentially expressed genes (DEGs) with $p\text{-adj} < 0.01$ and Log_2 fold change (Log_2FC) > 1 and < -1 has been performed using ClusterProfiler (v4.6.2) [14].

For single nucleotide variants (SNV) calling, filtered reads were aligned to the *Homo sapiens* reference genome (GENCODE release 36) using STAR v2.7.8a in two-pass mode.

For more details, refer to the additional supporting information (Additional file 1).

CRISPR/Cas9 genome editing

The silencing of PD-L1 in NSCLC-B cells was performed by using PD-L1 (CD274) Human Gene non-homology mediated CRISPR knock-out kit (KN413071; Origene, Rockville, MD, USA), according to the manufacturer's instructions. The kit contained two RNA guides and a linear donor DNA including genes for puromycin resistance and green fluorescence protein (GFP). TransIT-X2[®] Dynamic Delivery System MIR 6004 (Mirus Bio, Madison, WI, USA) was used for transfection. Cells were selected and maintained in 1 $\mu\text{g}/\text{mL}$ puromycin (Thermo Fisher Scientific), obtaining the two cell line clones NSCLC-B CL1 and NSCLC-B CL2, derived from NSCLC-B cells transfected with guide 1 and guide 2, respectively. The expression levels of PD-L1 and CD44 on the clones were measured by flow cytometry.

2D-growth and clonogenic assay

Cells were seeded in a 24-well plate at 0.2×10^5 cells/well in RPMI+10% FBS (for NSCLC-B and NSCLC-H cells) or RPMI+10% FBS + 1 $\mu\text{g}/\text{mL}$ puromycin (for NSCLC-B CL1 and NSCLC-B CL2 cells) for cell growth evaluation. The clonogenic assay was performed by seeding 400, 800 or 1600 cells/well in 6-well plates. After 7 days, cultures were fixed in 96% ethanol and stained with 0.05% crystal violet. Colonies, *i.e.* groups with more than 10 cells, were counted under an inverted microscope.

To assess cell sensitivity to IFN- γ and PD-L1 inhibition, NSCLC-B and NSCLC-H cells were seeded at 0.5×10^6 cells/ 25 cm^2 cell culture flasks in RPMI + 10% FBS. After 24 h, cells were treated with recombinant human IFN- γ (kindly provided by G. Garotta, F. Hoffmann-La Roche & Co., Basel, Switzerland) or anti-PD-L1 monoclonal antibody (mAb) atezolizumab (Tecentriq, Genentech), whose final concentrations are reported in figures or in figure legends. Cell growth and immunological modulation of MHC class I complex, PD-L1 and CD44 were assessed 72 h later by vital counting and cytofluorimetric analysis.

Soft-agar colony formation assay

For three-dimensional (3D)-soft-agar clonogenicity evaluation, NSCLC-B and NSCLC-H cells were seeded

at 200 cells/well in 24-well plates in semisolid medium consisting of RPMI + 10% FBS + 0.33% agar (Sea-Plaque Agarose, Lonza, Switzerland), with a 0.5% agarose underlay. For the assessment of cell line sensitivity to IFN- γ treatment or PD-L1 modulation in 3D culture conditions, NSCLC-B cells were seeded at 0.2×10^4 cells/well in 24-well plates in semisolid medium consisting of RPMI + 10% FBS + 0.33% agar, containing recombinant human IFN- γ , atezolizumab or only medium, with a 0.5% agarose underlay.

For the assessment of BoLC.8M3 sensitivity to IFN- γ treatment in 3D culture conditions, cells were seeded at 10 000 cells/well in 24-well plates in semisolid medium consisting of DMEM + 20% FBS + 0.33% agar, containing recombinant mouse IFN- γ (kindly provided by Dr. G.R. Adolf, Ernst-Boehringer Institute, Vienna, Austria), or only medium, with a 0.5% agarose underlay.

Colonies (diameter $> 90 \mu\text{m}$) were counted 2–3 weeks later under an inverted microscope in dark-field, as previously described [15]. NSCLC-B soft-agar colonies, grown in the presence of the previously described treatments or medium alone, were picked-up through a sterile pipette tip and subcultured in the same adherent conditions described for NSCLC-B and NSCLC-H cell lines. The derived cell lines were renamed as “bulk agar” cell lines, followed by the specific treatment that cells had received in soft-agar.

Sphere-forming assay

For the assessment of NSCLC-B and NSCLC-H sphere formation ability, cells were seeded at 0.1×10^5 cells in 4 mL of complete MammoCult medium (STEMCELL Technologies, Vancouver, Canada) without serum in 6-well Ultra-Low adherence plates (Corning Life Sciences), according to the MammoCult Human Medium Kit protocol. For the assessment of cell line sensitivity to IFN- γ treatment and PD-L1 modulation in sphere-formation assay, NSCLC-B cells were seeded at 500, 5 000 or 10 000 cells in 4 mL complete MammoCult medium. Recombinant human IFN- γ or atezolizumab were added to the medium at the concentrations reported in figures or in figure legends. Cells were incubated at 37°C in a humidified 5% CO_2 atmosphere for a week. Spheres, *i.e.* multi-cell structures with a diameter larger than 90 μm , were counted one week after seeding under an inverted microscope in dark field [11].

Establishment of organoids (tumoroids)

Approximately 0.3×10^5 cells were resuspended in Geltrex LDEV-Free Reduced Growth Factor (RGF) Basement Membrane Extract (BME) (Thermo Fisher Scientific), seeded in low adhesion 48-well plates (Greiner Bio-One, Kremsmünster, Austria), and, after domes

polymerization, an expansion medium was added. For the composition of the expansion medium, refer to the additional supporting information (Additional file 1). Organoids were disaggregated by gentle pipetting and incubation in cold PBS for 1 h on ice, every 14 days.

Immunofluorescence of organoids

NSCLC-H organoids were stained for Ki-67 and CD44. The organoids were gently removed from their matrix by incubation in cold PBS for 1 h and then fixed in cold 4% paraformaldehyde for 40 min at 4°C. Subsequently, cell structures were resuspended in PBS containing 0.1% Tween20 (Applichem, Darmstadt, Germany) for 10 min at 4°C and blocked for 1 h at room temperature in PBS containing 0.1% Triton X-100 and 2% bovine serum albumin (BSA) solution to minimize background non-specific staining. Then, the primary antibodies CD44 (clone IM7, 1:250, BioLegend, San Diego, CA, USA) and Ki-67 (clone SP6, 1:250, Thermo Fisher Scientific) diluted in PBS containing 0.1% Triton X-100 and 0.5% BSA were incubated overnight at 4°C on a shaker. After washing, 1 h incubation with the secondary antibodies (1:500, Thermo Fisher Scientific) goat anti-rat IgGAF555 (for CD44 staining) and goat anti-rabbit AF647 (for Ki-67 staining) was performed. Hoechst 33342 (1:8000, Thermo Fisher Scientific) was incubated for 20 min at room temperature in a dark room to counterstain nuclei. Confocal images were captured on a Leica SP8 inverted confocal microscope. To quantify the levels of CD44 and Ki-67 proteins, ImageJ/FIJI software was used. A total of 4-5 random images for each organoid structure were used for the quantification and the calculation of the mean and standard error of the mean (SEM).

Cytofluorimetric analysis

Harvested cells were analyzed by immunofluorescence and cytofluorimetric analysis, as previously described [15]. The following antibodies were used for direct and indirect immunofluorescence: anti-human PD-L1 (5 µg/mL, atezolizumab, Tecentriq, Roche or Selleck Chemicals, Houston, TX, USA), anti-human MHC class I (clone W6/32, 1:80, Sera-Lab), anti-mouse CD44PE or BV711 (clone IM7, 1:10, BioLegend), goat anti-human IgG secondary antibody FITC or AF674 (1:20, Thermo Fisher Scientific) and anti-mouse IgGAF488 (1:100, Thermo Fisher Scientific). Cell cycle analysis was performed by using the Phase-FlowT Alexa Fluor 647 BrdU Kit (BioLegend), according to the manufacturer's instructions, only performing the staining with 7-Aminoactinomycin D. Data were acquired by using CyFlow Space (Sysmex Partec, Görlitz, Germany) and BD FACS Lyric cytometer and analyzed by using FCS Express (De Novo Software, Glendale, CA, USA).

Western blot analysis

Protein extraction, quantification and Western blotting were performed as previously reported [16]. The effect of IFN-γ (Proteintech, Rosemont, IL, USA) or anti-PD-L1 mAb (atezolizumab, Selleck Chemicals) on NSCLC-B cells was evaluated after exposing cells to the treatment for 6 h. An untreated sample ran in parallel as a control. A sample of untreated NSCLC-H cells was also included in the analysis. The list of primary and secondary antibodies used for Western blot analyses is reported in Additional file 2: Table S1. Proteins were detected by the digital imaging system Azure C600 (Azure Biosystems, Dublin, CA, USA) and quantified through densitometric analysis of bands by Azure Spot software (Azure Biosystems).

Statistical analysis

Experimental *in vitro* conditions analyzed with statistical measures were repeated two times, at least. The number of samples and replicates is reported in figure legends. The two-tailed unpaired Student's *t*-test or One sample *t* test were performed according to assumptions of the tests and to the variance between the compared groups. For One sample *t* test, the mean of each analyzed group was compared to the hypothetical mean of 100. The significance of differences between *in vivo* growth curves was assessed by using the analysis of variance (ANOVA) and the post-hoc Bonferroni's multiple comparison tests, according to assumptions of the tests and the variance between the compared groups. Statistical analyses were performed with Prism 10 software (GraphPad software, La Jolla, CA, USA).

For additional details about Materials and Methods, refer to the additional supporting information described in Additional file 1.

Results

Patient clinical history and molecular data

A 64-year-old, former light smoker (10 pack/year) woman was diagnosed with stage IVA adenocarcinoma of the lung (pleura and pericardium). Tumor cells derived from pleural effusion at the time of diagnosis (Tdx) were positive for PD-L1 (tumor proportion score, TPS: 70%) and CD44 (31% of tumor cells were 2+ positive) (Fig. 1A). KRAS^{G12V} mutation was detected from the tumor sample obtained at Tdx through next generation sequencing (NGS) analysis. A second sample collected before treatment (baseline, Tb), consisting of pleural effusion and parietal pleura, was analyzed. On this second sampling obtained at the Tb point, CD44 expression was not identified in tumor cells but only in stromal components, while PD-L1 TPS staining was confirmed to be 70% (Fig. 1A). Additionally, tumor cells at both Tdx and Tb points were positive for TTF-1 and Ber-EP4 (data not

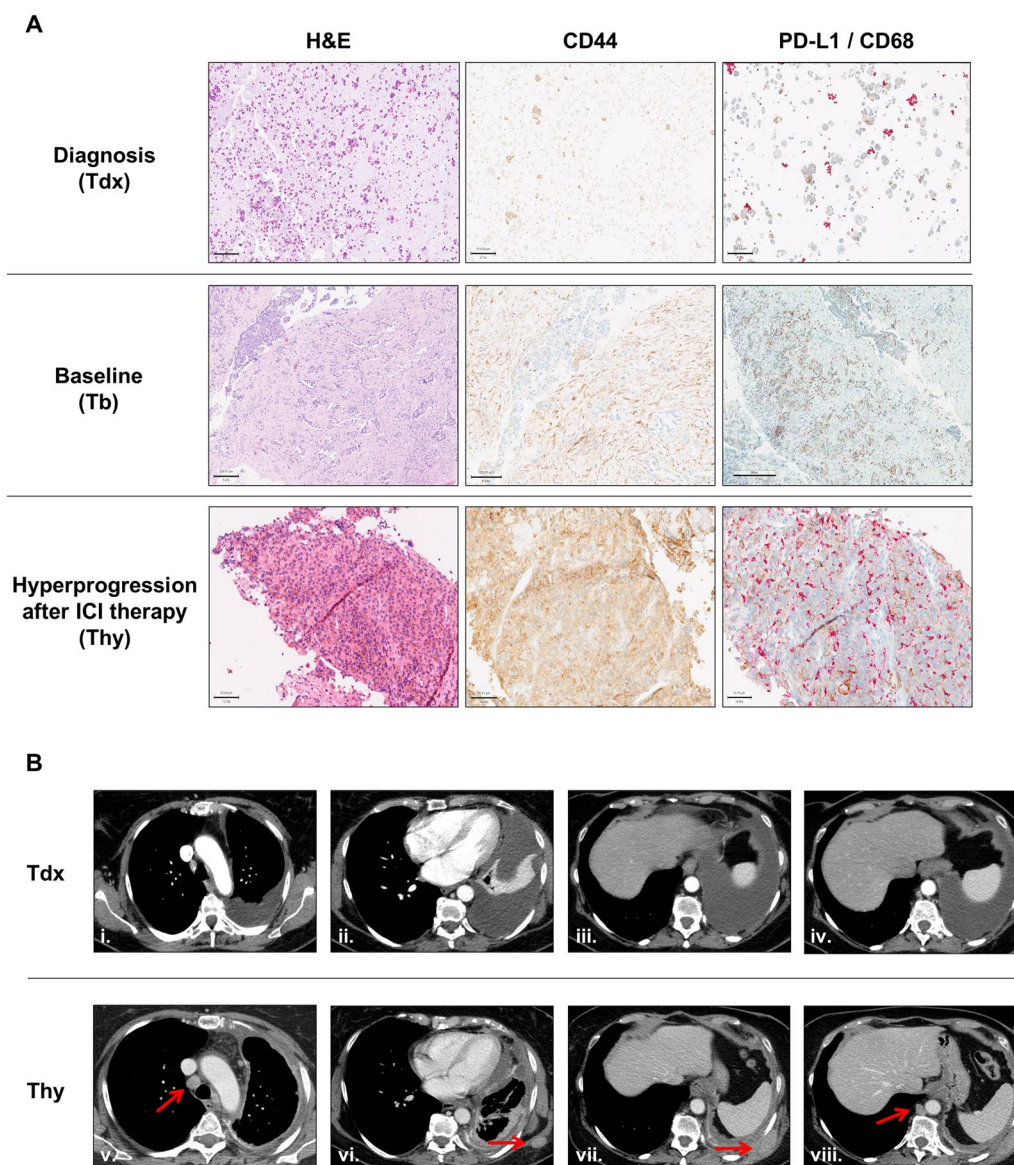


Fig. 1 Clinical features of patient’s tumor before and after ICI treatment. Time points: Tdx, time of the diagnosis; Tb, time of baseline; Thy, time of hyperprogression. **A** Hematoxylin and eosin staining (H&E) and CD44 and PD-L1 immunohistochemical staining of tumor samples. Tdx: pleural effusion; Tb: pleural biopsy; Thy: subcutaneous lesion. **Left:** H&E, black line from top to bottom: 313.30 μ m, 204.97 μ m and 92.60 μ m; **middle:** membrane CD44 expression on neoplastic cells, black line from top to bottom: 313.30 μ m, 120.01 μ m, 80.01 μ m; **right:** PD-L1 expression on tumor cells by double stain for PDL1 and CD68 (PD-L1: brown, CD68: red), black line from top to bottom: 139.24 μ m, 300 μ m and 61.73 μ m. **B** Imaging findings at the time of diagnosis (Tdx) (i.–iv.) and of progression to immunotherapy (Thy) (v.–viii.). Small right paratracheal lymph node (i.) progressed on immunotherapy (v., red arrow). Left pleural effusion (ii.) and left pleurodesis signs associated with the appearance of subcutaneous metastatic site (vi., red arrow). Left pleural effusion (iii.) and left pleurodesis signs associated with the appearance of a metastatic site at the left thoracic wall (vii., red arrow). Small right paraortic lymph node (iv.) progressed on immunotherapy (viii., red arrow). ICI: immune checkpoint inhibitors

shown). A first-line treatment with pembrolizumab was administered for 5 cycles. Radiological tumor assessment through computed tomography scans showed evidence of HPD, with metastatic tumor dissemination in soft tissue and thoracic wall other than in abdominal and thoracic lymph nodes (Fig. 1B). At this time, tumor cells collected

from a new subcutaneous biopsy (hyperprogression, Thy) maintained the expression of TTF-1 and Ber-EP4 (data not shown), together with PD-L1 (TPS: 65%) and CD44 (58% of tumor cells were 2+ positive) (Fig. 1A). Second-line treatment consisting of pembrolizumab, carboplatin and pemetrexed was administered, without any clinical

improvement. A third-line treatment with docetaxel was initiated without any clinical benefit and the patient died of further progressive tumor disease.

Establishment and characterization of NSCLC-B and NSCLC-H cell lines

To investigate the behavior of cancer cells at the time of baseline and at the time of hyperprogression, two primary cell cultures were established from tumor samples, obtained before ICI-based treatment initiation at the Tb point (NSCLC-B cell line) and at the time of radiological evidence of HPD under ICI treatment, *i.e.* Thy point (NSCLC-H cell line). KRAS^{G12V} mutation, previously identified in the tumor at the Tdx point, was also identified in both cell lines (Additional file 3: Table S2).

In adherent culture conditions, cell lines showed different morphology and behavior: while NSCLC-B formed a compact homogeneous monolayer of cells with polygonal morphology, NSCLC-H showed a less organized, stratified layer of cells (Fig. 2A). In addition, NSCLC-H cells showed the ability to generate organoids which, on the contrary, was not observed in NSCLC-B cell line (Fig. 2A). Of note, organoids were positive for CD44 and Ki-67 expression (Fig. 2B).

The behavior of NSCLC-B and NSCLC-H cell lines was further evaluated for comparison, both *in vitro* and *in vivo*. In general, NSCLC-H cells exhibited a significantly higher 2D and 3D-soft-agar clonogenicity and sphere-forming ability compared to NSCLC-B cells (Table 1). Furthermore, the NSCLC-H cell line was characterized by faster 2D-growth capacity, showing a significant decrease of cells in the G1 phase of the cell cycle compared to NSCLC-B cells (Table 1). Finally, patient-derived xenografts (PDX) derived from the tumor biopsy at the Thy point (NSCLC-H tumor) showed a faster growth compared to the PDX established from the tumor sample at the Tb point (NSCLC-B tumor) (Table 1).

Transcriptome analysis showed profound differences between NSCLC-H and NSCLC-B cells (PC1: 96% variance, Additional file 5: Figure S1A), evidencing 3525 genes differentially expressed between the two cell lines ($p\text{-adj} < 0.01$ and $\text{Log2FC} > 1$ or < -1), of which 1732 up-regulated and 1793 down-regulated in NSCLC-H cell line as compared to NSCLC-B (Fig. 2C). According to over representation analysis, up-regulated genes were involved in a plethora of biological processes (GO terms BP). Specifically, the top-20 GO terms BP evidenced enrichment in pathways of different cell types/tissues, including neural, epithelial, bone, muscle and connective tissues, suggesting a less differentiated status of NSCLC-H tumor cells compared to the NSCLC-B ones (Additional file 5: Figure S1B-i.). On the other hand, down-regulated genes in NSCLC-H cell line were associated with the

differentiative status of epithelial cells, supporting evidence of a partial epithelial-to-mesenchymal transition (EMT) in NSCLC-H cells (Additional file 5: Figure S1B-ii.). Up-regulated genes were enriched in molecular functions (GO terms MF), including channel activity and ion transportation, insulin-like growth factor binding and, in general, growth factors activity, carbohydrate and glycosaminoglycan binding (Additional file 5: Figure S1B-iii.). Down-regulated genes were enriched in molecular functions associated with cell-cell interactions and cytoskeletal binding, including actin filaments, laminin binding and DNA binding (Additional file 5: Figure S1B-iv.). GSEA analysis revealed clusters of genes, mainly up-regulated in the NSCLC-H cell line, involved in plasticity, tumor invasiveness and cell cycle (Fig. 2D).

In summary, phenotypical and functional characterization of our cell lines revealed more aggressive traits in the NSCLC-H model, compared to NSCLC-B. Transcriptome analysis of the cell lines also revealed a markedly different gene expression profile between the cell lines, evidencing the modulation of genes able to induce plasticity traits in the NSCLC-H cell model.

CD44 and CD44 isoforms

Among the differentially expressed genes, we focused our attention on CD44, a transmembrane glycoprotein with pleiotropic functions, which has been implicated in cancer progression, invasiveness, and plasticity [17]. Notably, CD44 was more expressed by NSCLC-H cells compared to NSCLC-B cells (Log2FC : 2.882, $p\text{-adj}$: 6.20E-49) (Fig. 2E and Additional file 6: Figure S2A). Moreover, the protein expression profile assessment of two additional NSCLC patient-derived cell lines, established from two ICI-treated patients at the time of HPD development (NSCLC-H2 and NSCLC-H3), also revealed elevated CD44 expression, consistent with the findings observed in the NSCLC-H cell line (Additional file 7: Figure S3A). In line with these observations, the assessment of CD44 expression changes in tumor samples from two further immunotherapy-resistant patients across the time points T0 (baseline) and T1 (resistance onset), also highlighted an evident increase in CD44 expression at T1 in both the clinical cases (percentage of CD44-positive tumor cells, case 1, T0: 38%, T1: 63%; case 2, T0: 13%, T1: 28%) (Additional file 7: Figure S3B).

These findings led us to hypothesize an association between CD44 expression and the development of resistance to immunotherapy, prompting us to further investigate CD44 in the context of ICI resistance.

Since, together with the standard isoform of CD44 (CD44s), multiple isoforms of CD44 have been reported in both normal and malignant cells [18], we specifically investigated the transcriptional profile of both the cell

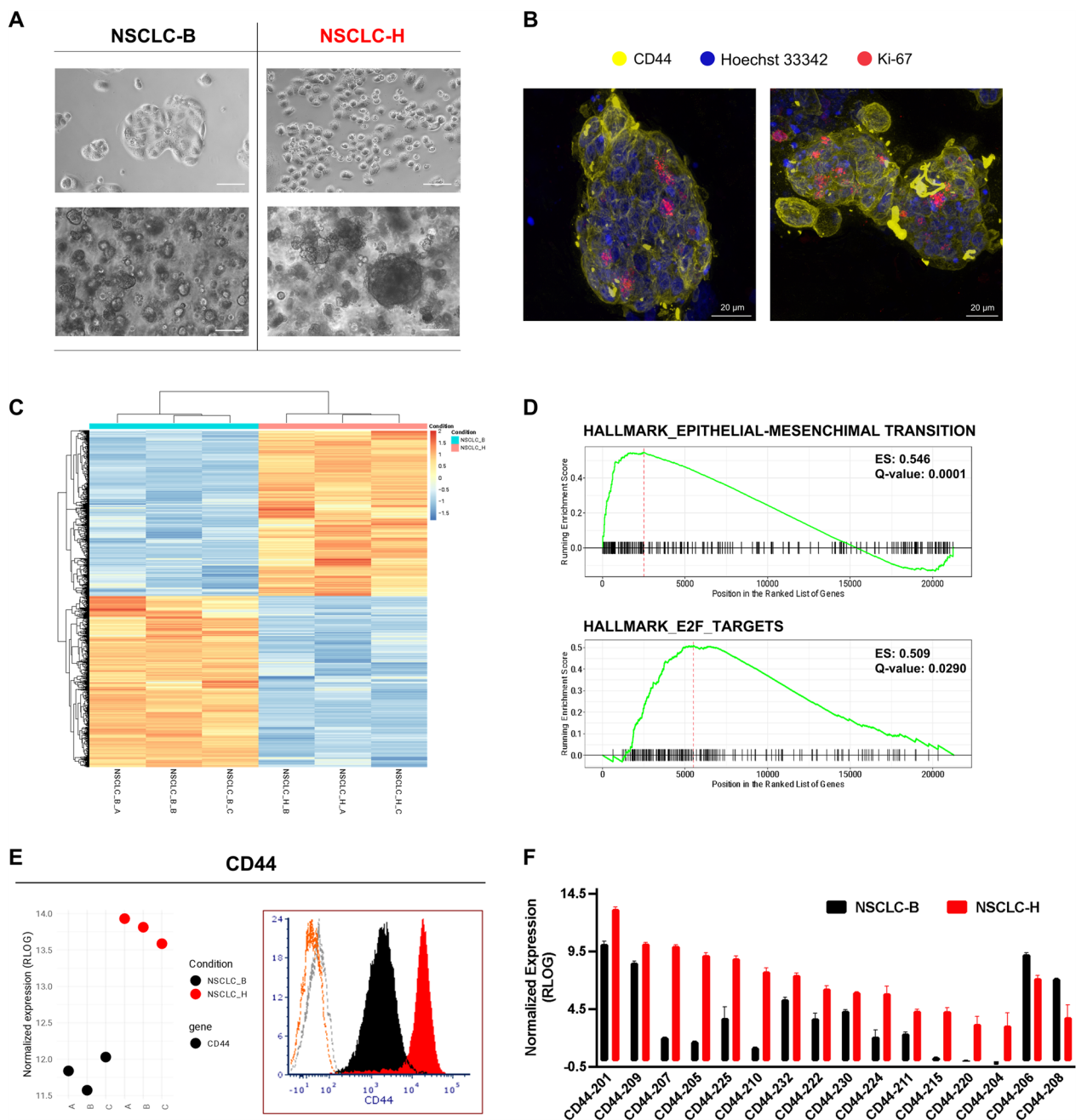


Fig. 2 Phenotypal, functional and transcriptomic characterization of NSCLC-B and NSCLC-H cell lines. **A** Morphology of NSCLC-B and NSCLC-H cells cultured under 2D conditions (**up**), or in matrigel with appropriate organoid medium (**down**), observed through an inverted microscope. White line corresponds to 100 μ m. **B** Representative confocal images of NSCLC-H cell line-derived organoids stained for CD44 (yellow) and the nuclear antigen Ki-67 (red) proteins. Nuclei were counterstained with Hoechst 33342 (blue). Scale bar: 20 μ m. Leica TCS SP8 Microscope, HC PL APO CS2 40 \times /1.30 OIL optical zoom 2.5 \times (left) or 2 \times (right) were used. Pixel-based quantification of CD44 and Ki-67 intensity in NSCLC-H cell line-derived organoids: left, CD44: 51.43 \pm 4.37 pixels, Ki-67: 13.77 \pm 2.09 pixels; right, CD44: 21.24 \pm 3.79 pixels, Ki-67: 9.00 \pm 1.73 pixels. **C** Heatmap showing the z-score of normalized expression values (RLOG) of differentially expressed genes (DEG, p-adj < 0.01 and Log2FC > 1 or < -1) in NSCLC-H vs NSCLC-B cells. **D** GSEA enrichment plots of curated lists related to plasticity, cell cycle and invasiveness. **E Left**: normalized expression (RLOG) of the *CD44* gene, as identified by RNAseq analysis; **right**: CD44 protein expression quantified by flow-cytometry (NSCLC-B, grey: unstained control, black: stained sample; NSCLC-H, orange: unstained control, red: stained sample). **F** Normalized expression (RLOG) of CD44 transcript isoforms, as identified by RNAseq analysis. Log2FC and p-adj of each transcript isoform in NSCLC-H vs NSCLC-B are reported in Additional file 4: Table S3. 2D: two-dimensional

Table 1 Growth-related features of NSCLC-B and NSCLC-H cell lines or tumors

	NSCLC-B	NSCLC-H	p-value
2D-growth (cell population doublings-168 h)	2.92±0.04	4.01±0.16	< 0.01
2D-clonogenicity (%)	1±1%	29±1%	< 0.001
3D-soft-agar clonogenicity (%)	0.15±0.05%	18.15±0.50%	< 0.001
Sphere formation ability (number of spheres)	51±2	82±5	< 0.05
Cells in the G1 phase of the cell cycle (%)	63±3%	47±2%	< 0.01
PDX tumor growth rate (doubling time-weeks)	1.430±0.154	0.562±0.104	< 0.05

Statistical analysis: Student's t-test (n=2-3)

lines for CD44 variants, evidencing a different pattern of CD44 transcript expression between the cell line models. CD44 transcript isoforms showed differential abundance in NSCLC-H vs NSCLC-B cell line (Fig. 2F, Additional file 8: Figure S4A) and their level of expression ranged from low (Transcripts Per Kilobase Million, TPM < 3) to high (TPM > 10) levels (Additional file 4: Table S3). NSCLC-H cell line mainly showed increased levels of the short transcript isoforms CD44-201 (CD44s), CD44-205, CD44-209, CD44-222 and CD44-230 (Fig. 2F). Other transcript isoforms more abundant in NSCLC-H cells compared to NSCLC-B cells included CD44-204, CD44-211, CD44-220 and CD44-224. In addition, NSCLC-H cell line also showed increased levels of two transcripts with a premature translation termination codon (CD44-207 and CD44-210) and three transcripts unable to be translated due to intron retaining (CD44-215, CD44-225 and CD44-232), compared to NSCLC-B cell line (Fig. 2F). Interestingly, although total CD44 transmembrane protein was more highly expressed in NSCLC-H cells compared to NSCLC-B cells, longer transcripts of the protein, such as CD44-206 (CD44v6) and CD44-208 (CD44v2-v10), were more abundant in NSCLC-B cell line than NSCLC-H (Fig. 2F). As a complementary approach, we also performed differential exon usage analysis, which confirmed the higher usage of exons belonging to the short isoforms (e2, e5-e6, e20-e23 and e25) in NSCLC-H cells as compared to NSCLC-B cells, which, in contrast, utilized more e7-e9 and e11-e19 exons, which are present in the long CD44 isoforms (Additional file 8: Figure S4B).

Collectively, our data heavily suggest an association between CD44 expression and resistance to ICIs. Moreover, transcriptomic data also evidenced a different expression pattern of CD44 transcripts between

NSCLC-B and NSCLC-H cell lines, highlighting an association between the short CD44 isoforms and immunotherapy resistance.

Cellular response to immune components

The tumor microenvironment (TME) plays a relevant role in the therapeutic response to ICIs. Thus, we indirectly evaluated the interaction of cancer cells with immune components of the TME by analyzing the activation of immune-related pathways and the expression of molecules involved in ICI response.

PD-L1 is a transmembrane glycoprotein involved in immune response inhibition and tumor immune evasion, representing one of the most common targets for immune checkpoint blockers [3]. The evaluation of key proteins involved in tumor-immune interactions evidenced a down-modulation of PD-L1 expression in NSCLC-H cell line compared to NSCLC-B (Fig. 3A, Additional file 6: Figure S2B). Moreover, GSEA analysis showed that the “inflammatory response” Hallmark gene set was significantly up-regulated in the NSCLC-H model, compared to the NSCLC-B one (Fig. 3B). Furthermore, a subgroup of enriched score genes associated to GSEA analysis and related to the cellular response to IFN-γ and interferon-alpha (IFN-α) was down-regulated in NSCLC-H cells compared to NSCLC-B cells (Fig. 3C). On the contrary, genes associated with interferon-beta (IFN-β) cellular responses were up-regulated in NSCLC-H cells, together with genes involved in IL-6/JAK/STAT3 signaling (Fig. 3C, Additional file 5: Figure S1C).

Additionally, two molecules that have been associated with reduced T cell responsiveness, namely NDRG1 and ADORA1 [19, 20], resulted to be significantly overexpressed by the NSCLC-H cell line, compared to NSCLC-B cells (Additional file 5: Figure S1D).

Investigating the activation of molecular pathways associated with response to inflammatory stimuli and cell proliferation, we observed an increased activation of STAT1, JAK2 and IRF3 in NSCLC-H compared to NSCLC-B cells, while, on the contrary, a reduced tyrosine phosphorylation of STAT3 was observed in NSCLC-H cell line (Fig. 3D, Additional file 9: Figure S5). Interestingly, the ERK/MAPK pathway was more activated in the hyperprogressive cell line compared to the baseline one (Fig. 3D, Additional file 9: Figure S5). Moreover, IFNGR1 resulted to be overexpressed in the NSCLC-H cell line compared to the NSCLC-B one (Fig. 3D). Of note, variant calling from RNAseq data revealed the presence of 38 genes with pathogenic or predicted pathogenic single nucleotide variants (SNV) shared by both NSCLC-B and NSCLC-H cells (Additional file 3: Table S2). These SNV

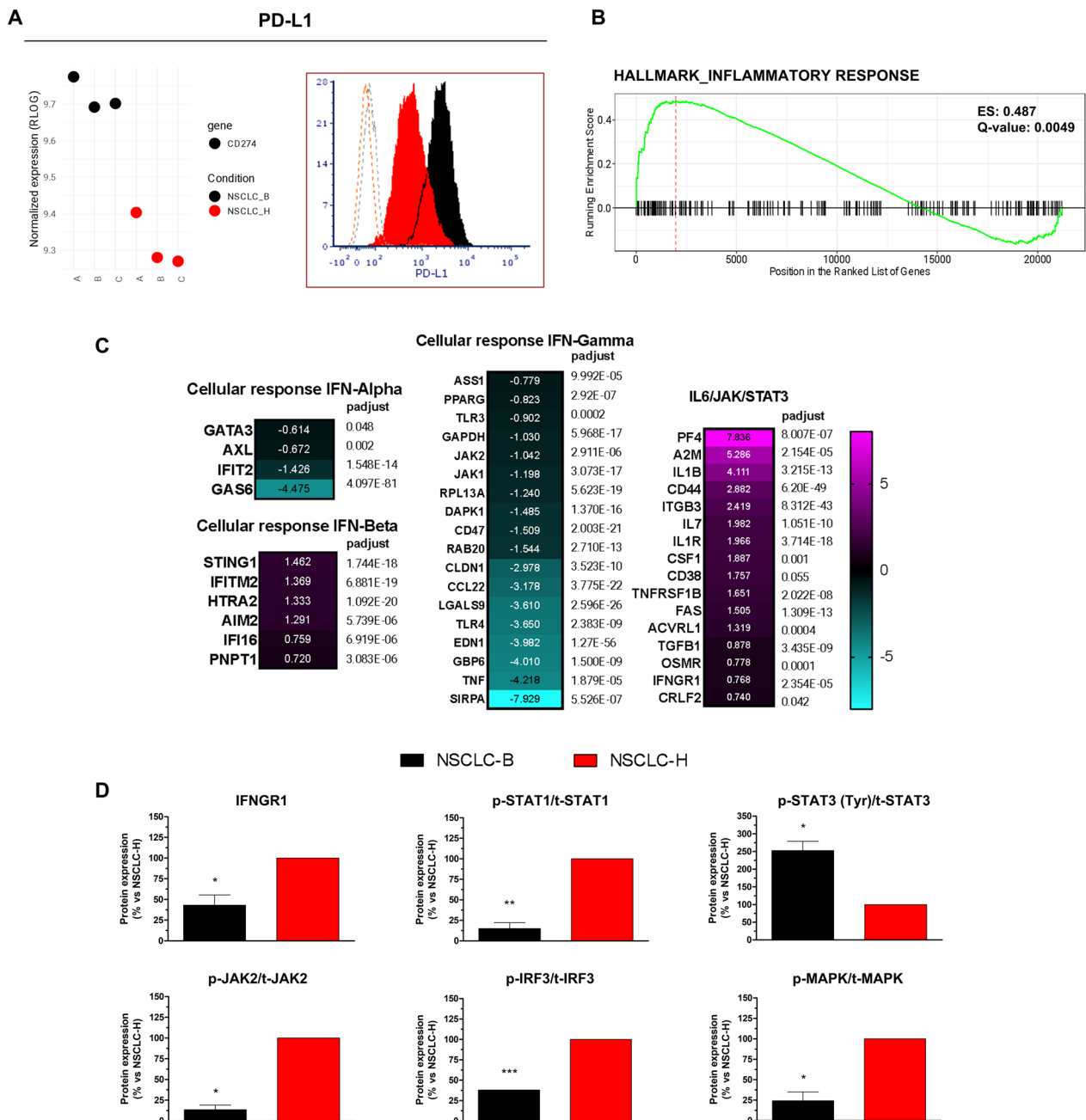


Fig. 3 Comparison of immune-related genes and proteins between NSCLC-B and NSCLC-H cell lines. **A** Normalized expression (RLOG) of *PD-L1* (CD274) gene, as identified by RNAseq analysis (Log2FC: -0.589, p-adj: 0.0003), and validation by flow cytometry (NSCLC-B, grey: unstained control, black: stained sample; NSCLC-H, orange: unstained control, red: stained sample). **B** GSEA analysis of curated list related to inflammatory response. **C** Heatmap showing the Log2FC of a subgroup of enriched score genes associated to GSEA analysis and reported in Additional file 5: Figure S1C, which are involved in immune-related cellular responses. Log2FC of differentially expressed genes in NSCLC-H compared to NSCLC-B is reported in the box and p-adj is reported on the right. **D** Western blot analysis for proteins involved in response to inflammatory stimuli and cell proliferation (n = 3, except for p-JAK2/t-JAK2 and p-IRF3/t-IRF3, in which n = 2). *p < 0.05, **p < 0.01, ***p < 0.001 by One Sample t test (each group vs theoretical mean of 100). Each bar represents mean with SEM. SEM: standard error of the mean

affected *TP53* and *JAK2* genes, known to be involved in the mechanisms of ICI resistance.

In summary, NSCLC-H cell line showed increased activation of pathways related to inflammation, IFN-β

signaling and cell growth as compared to NSCLC-B cells, together with up-regulation of genes involved in the inhibition of T-cell-mediated immune response.

In vitro response of NSCLC-B and NSCLC-H cell lines to IFN-γ

The mechanism of action of ICIs is based on the enhancement of T-cell activation and reversal of T-cell exhaustion through the targeting of immune checkpoints. IFN-γ, which exerts antiproliferative, cytostatic, pro-apoptotic and immunogenic effects on tumor cells, is believed to mediate the antitumor effect of cytotoxic T-cell populations, restored by ICI therapy [21]. Thus, we evaluated the effect of IFN-γ on NSCLC-B cells in vitro, mimicking the interaction between the baseline tumor cells and the anti-tumor cytokine released by reactivated cytotoxic T cells occurred in the patient at the moment of ICI treatment initiation. In adherent culture conditions, NSCLC-B cells were resistant to the antiproliferative effect of IFN-γ (Table 2). Furthermore, IFN-γ did not up-regulate the expression of PD-L1 or IFNGR1, while retaining its ability to induce MHC class I expression in NSCLC-B cells (Table 2). Similar effects were also observed on NSCLC-H cells in the presence of IFN-γ (Table 2). Western blot analysis of NSCLC-B cell line grown in adherent conditions in the presence of IFN-γ revealed increased activation of STAT1,

STAT2, JAK1, IRF9 and MAPK (Fig. 4A, Additional file 9: Figure S5).

In 3D culture conditions, IFN-γ surprisingly exerted a growth stimulating effect on NSCLC-B cells, inducing a significant increase in the number of soft-agar colonies (Fig. 4B). “Bulk agar” cell lines were established from 2D-subcultured soft-agar colonies (Fig. 4C). Interestingly, only “bulk agar” cells derived from colonies grown in the presence of low-dose IFN-γ showed increased CD44 expression, which was also accompanied by a partial change in cell morphology (Fig. 4C). Accordingly, sphere formation assay showed a significant increase of sphere production only in the presence of a low dose of IFN-γ (Fig. 4D).

Considering the atypical response of the NSCLC-B cell model to IFN-γ under 3D culture and the critical role that the *KRAS* mutation and p53 knockout have been reported to exert in ICI resistance [22], we also assessed the behavior of a transgenic murine lung adenocarcinoma cell line, namely BoLC.8M3, harboring the human *KRAS*^{G12D} mutation and that was knock-out for p53, under the same conditions. Interestingly, the BoLC.8M3 cell line not only demonstrated increased proliferation in the presence of IFN-γ under 3D culture conditions, consistent with the behavior of the NSCLC-B cell model, but it also exhibited partially accelerated tumor growth when injected into immunocompetent mice treated with the anti-PD-L1 monoclonal antibody (mAb) atezolizumab (Fig. 5A,B).

Collectively, these data suggest a hypo-functioning of canonical IFN-γ signaling in both NSCLC-B and NSCLC-H cell lines, as demonstrated by the absence of an IFN-γ-dependent antiproliferative effect in 2D culture conditions and PD-L1 induction on these cells. Rather, in vitro evidence suggests a pro-growth effect exerted by IFN-γ on 3D-cultured NSCLC-B cells, together with a direct regulation of CD44 expression, observed only in

Table 2 Response of NSCLC-B and NSCLC-H cell lines to IFN-γ in 2D culture conditions

	NSCLC-B	NSCLC-H
2D-growth (% over control)	100±3	88±9
PD-L1 expression (% over control)	114±7	109±17
MHC-I expression (% over control)	210±3	155±39
IFNGR1 expression (% over control)	83±3	84±2

IFN-γ: 7–10 ng/mL. For each cell line, n=2

(See figure on next page.)

Fig. 4 In vitro response of NSCLC-B cell line to IFN-γ. **A** Western blot analysis for proteins involved in IFN signaling and in cell growth on NSCLC-B cells treated with different doses of IFN-γ in 2D culture conditions (n=3–5, except for p-STAT3(Tyr)/t-STAT3, in which n=2). *p<0.05 by One Sample t test (each group vs theoretical mean of 100). Each bar represents mean with SEM. **B** NSCLC-B soft-agar colony formation in the presence of low (0.1 ng/mL) and high (100 ng/mL) doses of IFN-γ (n=6, three experiments—circle, triangle, square—each one with two technical replicates). *p<0.05 by One sample t test (each group vs theoretical mean of 100). Each bar represents mean with SEM. Each dot represents a replicate. **C** Morphological and phenotypical characterization of NSCLC-B “bulk agar” cell lines obtained from 2D-subcultured agar colonies grown in the presence of IFN-γ. **First line:** representative pictures of NSCLC-B soft-agar colonies grown without any treatment or in the presence of IFN-γ, observed through an inverted microscope in dark-field. To improve the visual appearance of the images, photos were converted into grayscale; **second line:** morphologies of NSCLC-B “bulk agar” cell lines cultured under 2D-adherent conditions, observed through an inverted microscope. White line corresponds to 100 μm. To improve the visual appearance of the images, photos were converted into grayscale and contrast and brightness were enhanced (+40% and +10%, respectively); expression of CD44 (**third line**) and percentage of CD44⁺ cells (**bottom**) on NSCLC-B “bulk agar” cell lines cultured under 2D-adherent conditions, measured by cytofluorimetric analysis (M1: marker) (n=3). ***p<0.001 by Student’s t-test. Each bar represents mean with SEM. **D** NSCLC-B sphere formation in the presence of low (0.1 ng/mL) and high (100 ng/mL) doses of IFN-γ (untreated and IFN-γ 0.1 ng/mL: n=14, seven experiments—different symbols—, each one with two technical replicates; IFN-γ 100 ng/mL: n=12, six experiments, each one with two technical replicates). *p<0.05 by One sample t test (each group vs theoretical mean of 100). Each bar represents mean with SEM. Each dot represents a replicate. SEM: standard error of the mean

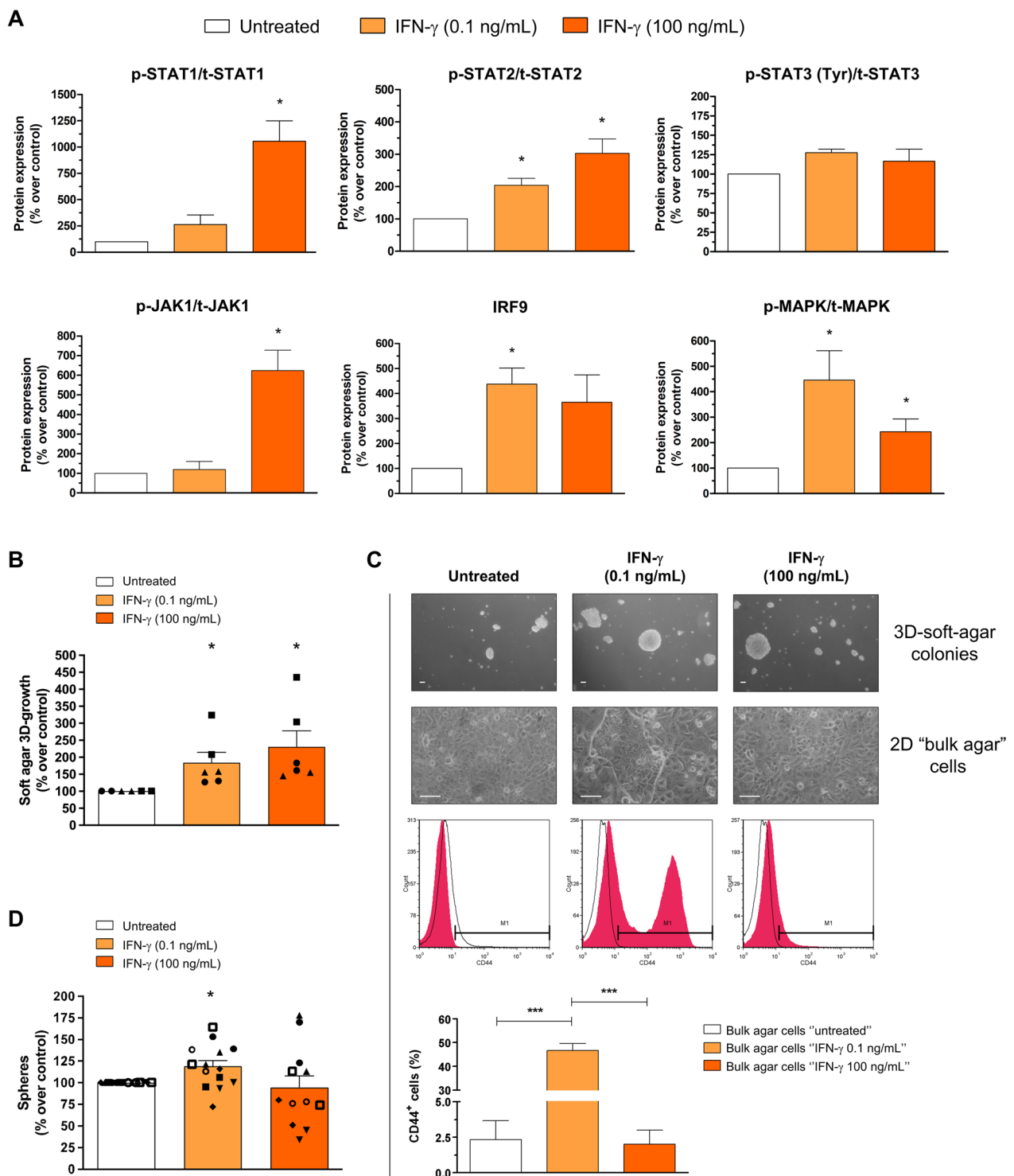


Fig. 4 (See legend on previous page.)

the presence of low doses of the cytokine. Preliminary studies conducted on the BoLC.8M3 murine transgenic cell line further support the association between atypical tumor responses to IFN- γ and ICI resistance.

PD-L1 modulation on NSCLC-B cell line

PD-L1 is known to have pro-tumoral functions not necessarily dependent on its interaction with the PD-1 receptor [23]. Several studies have indeed demonstrated

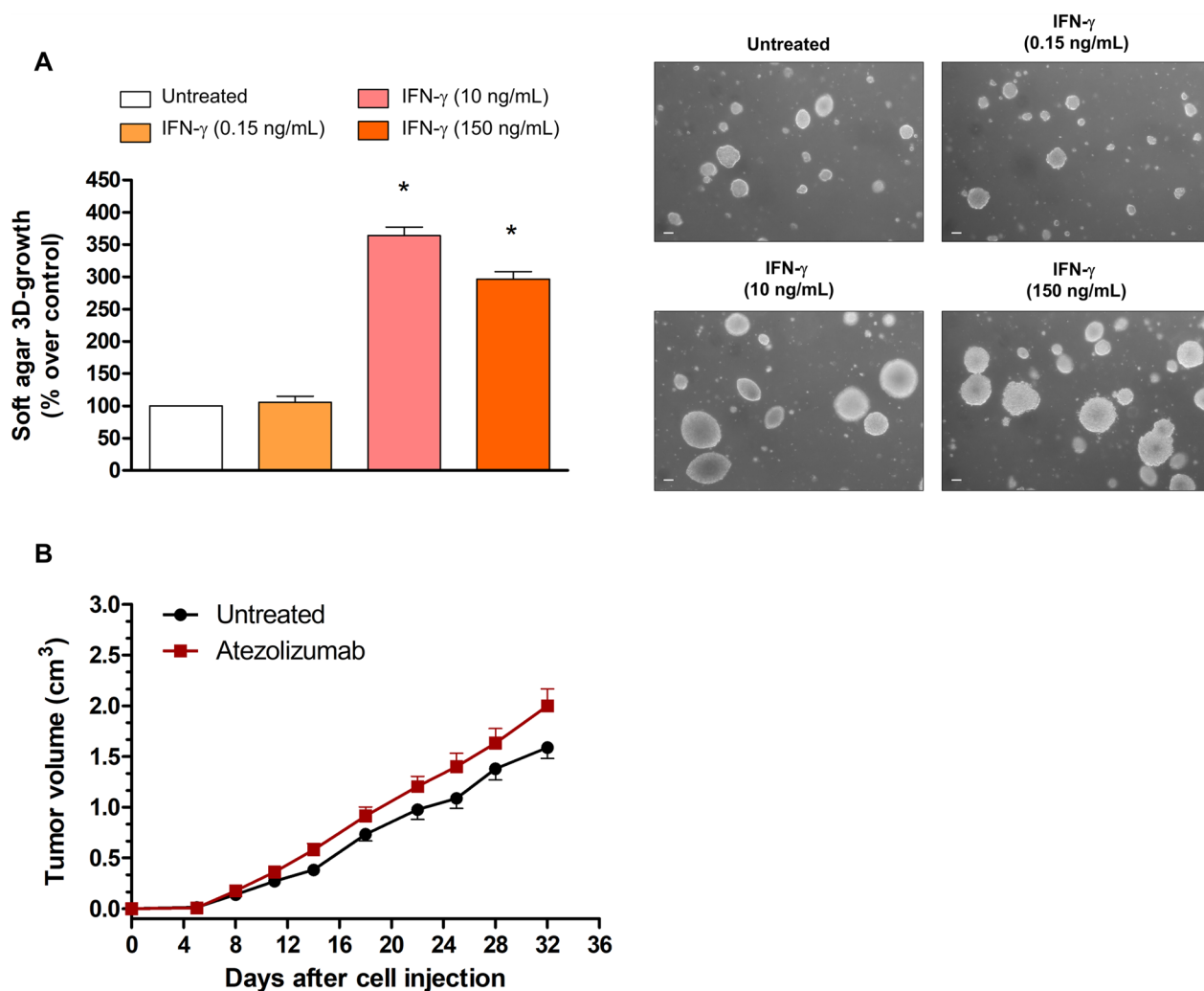


Fig. 5 Response of the BoLC.8M3 cell line to different doses of IFN- γ or atezolizumab. **A** BoLC.8M3 soft-agar colony formation in the presence of different doses of IFN- γ (n = 2). *p < 0.05 by One sample t test (each group vs theoretical mean of 100). Each bar represents mean and SEM. **Right:** representative pictures of BoLC.8M3 soft-agar colonies grown without any treatment or in the presence of IFN- γ , observed through an inverted microscope in dark-field. White line corresponds to 100 μ m. **B** Tumor growth of subcutaneously (s.c.) injected BoLC.8M3 cells in BALB/c mice treated with atezolizumab 10 mg/Kg, starting 1 day after cell injection (n = 15), or in untreated mice (n = 15). Two-way ANOVA was used to compare the groups (interaction, p < 0.01; treatment, p = 0.07). Day 32nd after cell injection: **p < 0.01 by Bonferroni's post-test (comparison between group means). Each point represents mean and SEM. SEM: standard error of the mean

the existence of a PD-1-independent intracellular signaling of PD-L1 in tumor cells [24–27]. Hence, we evaluated the effect of PD-L1 modulation on the NSCLC-B cell line. First, PD-L1 was targeted by the mAb atezolizumab in 3D culture conditions. The blockade of PD-L1 showed no significant effect on NSCLC-B growth in 3D-soft-agar assay (Fig. 6A). Despite this, the inhibition of PD-L1 not only promoted a change in cell morphology in colony-derived “bulk agar” cells, but it also significantly increased CD44 expression on tumor cells, compared to control (Fig. 6B). Accordingly, atezolizumab also significantly increased NSCLC-B capacity of forming spheres

(Fig. 6C). Preliminary studies of intracellular pathways influenced by PD-L1 blockade in NSCLC-B cells were carried out through Western blot analyses, highlighting an increase in the activation of MAPK in the presence of atezolizumab (Fig. 6D and Additional file 9: Figure S5). To further explore the role of PD-L1 modulation in cell behavior, we isolated two clones (NSCLC-B CL1 and NSCLC-B CL2) from NSCLC-B cells, previously transfected with a CRISPR/Cas9 guide designed to silence PD-L1 encoding gene. Both clones showed a decrease in PD-L1 expression compared to the NSCLC-B parental cell line (Additional file 10: Figure S6A). Surprisingly,

not only decreased expression of PD-L1 resulted in increased expression of CD44, leading to an expression profile similar to that of NSCLC-H cells, but a change in cell morphology, which became more similar to that of NSCLC-H cells, was also observed in the clones (Fig. 6E). In addition, NSCLC-B CL1 and CL2 cells also showed an evident increase in in vitro growth rate, which was comparable or even higher than the one of NSCLC-H cells (Fig. 6F and Additional file 10: Figure S6B).

Together, these data suggested that PD-L1 on NSCLC-B cells directly regulates CD44 expression and that its inhibition leads to increased tumor cell growth, both in 3D anchorage-independent and 2D cell culture assays, suggesting a relevant role of PD-L1 in both cancer cell stemness modulation and tumor growth.

Discussion

Despite the significant breakthrough provided by ICIs in the landscape of NSCLC treatment, the development of primary and secondary resistance highly hinders the therapeutic efficacy of ICI-based therapy [5]. Hyperprogressive disease (HPD) is a paradoxical acceleration of tumor growth induced by ICI-based treatment [6], whose molecular mechanisms and predictive biomarkers underlying this phenomenon are still unknown [7].

In this paper, we present a unique HPD preclinical model based on two cell lines established from NSCLC samples of the same patient collected before initiation of any treatment (NSCLC-B) and at the time of HPD occurrence on ICI therapy (NSCLC-H). NSCLC-H cells not only showed a profound transcriptome shift, but also exhibited increased stemness-like and pro-growth traits, together with increased expression of factors known to

be involved in tumor cell plasticity and stemness, including CD44 [28, 29]. This was particularly noteworthy since elevated expression of this protein was also observed on two additional patient-derived cell lines (NSCLC-H2 and NSCLC-H3), both established from tumor samples of two distinct ICI-treated patients who developed hyperprogression. Notably, an increase in CD44 expression was also observed on tumor samples of two further ICI-resistant patients across the time points of diagnosis and resistance development. In accordance with our observations, in their enlightening work, Li and colleagues also reported increased expression of CD44 in the ICI-treated tumors of their HPD syngeneic murine model, confirming an association between increased tumor CD44 expression and HPD onset [30].

Of note, the presence of several CD44 isoforms has been well documented in cancer and Gaiteiro and colleagues recently characterized the CD44 splicing code associated with bladder cancer, combining splicing analysis with glycome analysis [18, 31]. Our preliminary data, which still warrant definitive confirmation by other methods, revealed distinct transcriptional profiles for CD44 isoforms between NSCLC-H and NSCLC-B cell lines. While NSCLC-H showed an enrichment of short transcripts lacking several exons of the variable region of the protein, NSCLC-B showed instead increased presence of long isoform transcripts, including CD44v6 (CD44-206), CD44v2-v10 (CD44-208), and CD44s (CD44-201) variants [32]. Unfortunately, the role and impact of these distinct CD44 isoforms on tumor progression and therapeutic response are not well defined and hugely vary between different tumor types [17]. Hence, the different expression patterns of CD44

(See figure on next page.)

Fig. 6 Response of NSCLC-B cell line to PD-L1 modulation in 2D and 3D culture conditions. **A** NSCLC-B soft-agar colony formation in the presence of atezolizumab 10 µg/mL (n=6, three experiments—circle, triangle, square—, each one with two technical replicates). Each bar represents mean with SEM. Each dot represents a replicate. **B** Morphological and phenotypical characterization of NSCLC-B “bulk agar” cell lines obtained from 2D-subcultured agar colonies grown in the presence of atezolizumab 10 µg/mL. **First line:** representative pictures of NSCLC-B soft-agar colonies grown without any treatment or in the presence of atezolizumab, observed through an inverted microscope in dark-field. To improve the visual appearance of the images, photos were converted into grayscale; **second line:** morphologies of NSCLC-B “bulk agar” cell lines cultured under 2D-adherent conditions, observed through an inverted microscope. White line corresponds to 100 µm. To improve the visual appearance of the images, photos were converted into grayscale and contrast and brightness were enhanced (+40% and +10%, respectively); expression of CD44 (**third line**) and percentage of CD44⁺ cells (**bottom**) on NSCLC-B “bulk agar” cell lines cultured under 2D-adherent conditions, measured by cytofluorimetric analysis (M1: marker) (n=4). **p < 0.01 by Student’s t-test. Each bar represents mean with SEM. **C** NSCLC-B sphere formation in the presence of atezolizumab 10 µg/mL (n=18, nine experiments—different symbols—, each one with two technical replicates). ***p < 0.001 by One sample t test (group vs theoretical mean of 100). Each bar represents mean with SEM. Each dot represents a replicate. **D** Assessment of MAPK activation in NSCLC-B cells treated with atezolizumab (5 µg/mL) in 2D-adherent culture conditions, as measured by Western blot analysis (n=4). Each bar represents mean with SEM. **E** Comparison of morphological and phenotypical features between NSCLC-B CRISPR-engineered cell lines (NSCLC-B CL1 and NSCLC-B CL2), NSCLC-B and NSCLC-H cell lines. **Up:** representative photos of NSCLC-B, NSCLC-B CL1, NSCLC-B CL2 and NSCLC-H cell lines, observed through an inverted microscope in dark-field. White line corresponds to 100 µm; **bottom:** expression of CD44 on NSCLC-B (black), NSCLC-B CL1 (green), NSCLC-B CL2 (dark green) and NSCLC-H (red) cell lines cultured under 2D-adherent conditions, measured by cytofluorimetric analysis. **F** Comparison of 2D-clonal efficiency between NSCLC-B, NSCLC-B CL1, NSCLC-B CL2 and NSCLC-H cell lines (n=6). ***p < 0.001 by Student’s t-test. Each bar represents mean with SEM. 2D: two-dimensional, SEM: standard error of the mean

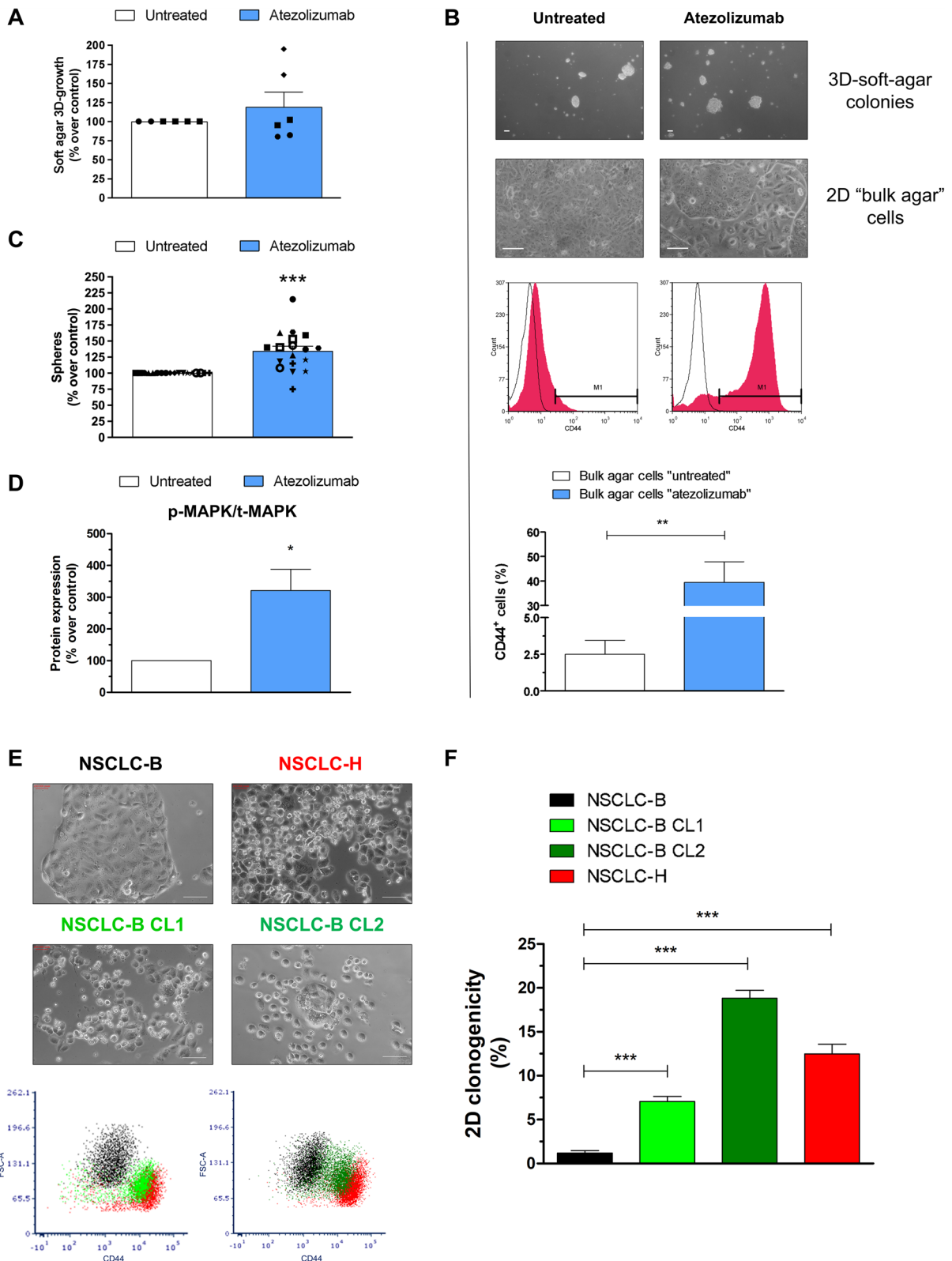


Fig. 6 (See legend on previous page.)

transcript isoforms in NSCLC-B and NSCLC-H will deserve further investigations.

The major role played by IFN- γ , released by reinvigorated T cells, and PD-L1 in tumor response to ICI therapy, encouraged us to investigate the in vitro response of NSCLC-B to IFN- γ and to PD-L1 modulation. PD-L1 is currently the only validated predictive biomarker used for the selection of patients eligible for anti-PD-(L)1 therapy [33]. Beyond the established immunosuppressive role of the PD-L1/PD-1 interaction, a PD-L1 activity independent of PD-1 binding has been reported and associated with cancer survival, as an ambivalent player [23, 24, 34–36]. Moreover, the involvement of PD-L1 in plasticity modulation and CD44 expression of both cancer cells and macrophages has also been documented and associated with epigenetic changes [37–43]. In our cell line model, PD-L1 showed a role in tumor plasticity regulation: the modulation of PD-L1 expression in NSCLC-B cells not only increased CD44 cell surface expression, but also resulted in alterations in cellular morphology and increased in vitro growth properties.

For what concerns IFN- γ tumor response, previous studies reported that the dose of 10 ng/mL of IFN- γ was able to induce a strong antiproliferative effect (cell survival rate < 30%) and PD-L1 induction in vitro in human cancer cells classified as highly sensitive to IFN- γ [44, 45]. NSCLC-B cell model showed no inhibition in cell growth and no induction of PD-L1 expression when treated with a similar dose of IFN- γ . Notably, the disruption of the IFN- γ signaling pathway in tumor cells has been increasingly recognized as a significant mechanism contributing to the resistance to ICIs [46]. Moreover, the NSCLC-B cell line also exhibited a highly atypical response to IFN- γ , consisting of the cross-activation of mediators of the type-I IFN pathways—including STAT2 and IRF9—, increased cell proliferation in 3D culture settings and induction of CD44 expression. On the other hand, NSCLC-H showed a down-regulation of genes involved in the cellular response to IFN- γ and increased activation of genes involved in IFN- β signaling pathway. While there is a notable interplay between the IFN- γ signaling pathway and type I-IFN pathways, due to the sharing of common mediators including STAT1 and JAK2, each pathway is characterized by its own distinct mediators and functions, contributing to the complex regulation of immune responses [47, 48]. Of note, an increased activity of the IFN-related transcription factor STAT1 has also been reported in tumor samples of ICI-resistant patients and in the B16 cell model in the presence of persistent stimulation of IFN- γ signaling [49, 50]. Accordingly, we observed increased STAT1 activation in the NSCLC-H cell line model, compared to NSCLC-B cells. The atypical activation of

type I-IFN pathway mediators by IFN- γ in the NSCLC-B model may suggest an unexplored crosstalk between these pathways, which, to the best of our knowledge, has not been previously documented in the literature in the context of tumor resistance to ICIs. In fact, existing reports have highlighted the ability of IFN- γ to induce non-canonical transcriptional complexes that resemble the ones of type I-IFN pathways [51, 52]. Interestingly, the activation of type I-IFNs signaling pathways have been reported to reduce cell responsiveness to IFN- γ by reducing the expression of cell surface IFNGR1 [53, 54]. In line with these data, IFNGR1 was not induced in NSCLC-B cells after IFN- γ treatment. In addition, the exposure of NSCLC-B cells to IFN- γ also significantly activated the pro-proliferative MAPK pathway, which has been reported to be triggered by both IFN- γ and type I IFNs, and to promote the induction of CD44 expression [55–57]. Lastly, consistently with our findings, evidence of an involvement of type I-IFN signaling in tumor resistance to immunotherapy has also been reported [49, 50]. Alterations of both type I and type II-IFN signaling pathways have been indeed documented in NSCLC patients who developed ICI resistance [58]. All this evidence supports our findings and suggests the presence of an uncanonical IFN- γ signaling pathway overlapping with the one of type I IFNs, able to modulate cancer stemness and plasticity, leading to ICI resistance. This is demonstrated by the atypical response to IFN- γ observed in the NSCLC-B model, and further corroborated by the unexpected, pro-growth effect of IFN- γ on our preclinical model of ICI resistance, represented by the transgenic *KRAS*-mutated and p53 knock-out BoLC.8M3 murine cell line.

Regarding IFN- γ -mediated CD44 expression, it is important to mention that only low-doses of the cytokine induced the expression of this marker in the NSCLC-B model. These data are in accordance with the findings of Song and colleagues, who demonstrated that low doses of IFN- γ trigger the activation of an alternative signaling pathway mediated by ICAM1 in NSCLC cell lines, subsequently leading to increased cancer stemness [59]. Although the mechanisms underlying the behavior of NSCLC-B model in the presence of IFN- γ are not yet understood and require further investigation, it is possible to hypothesize that IFN- γ may activate alternative pathways depending on the dose, including ICAM1 pathway, resulting in a modulation of tumor plasticity, as demonstrated by Song and colleagues [59]. Indeed, some evidence suggesting that IFN- γ might modulate tumor stemness and plasticity in different tumor types already exists in the literature [44, 60]. Of note, cancer plasticity may not only enhance tumor aggressiveness, but also

promote an immune-suppressive tumor microenvironment (TME), further fueling cancer cell proliferation [61].

The observation that PD-L1 modulation could elicit effects similar to those induced by IFN- γ in NSCLC-B cells, both in terms of cell growth stimulation and CD44 increased expression, is particularly intriguing, as it suggests the existence of an unknown molecular circuit between IFN- γ and PD-L1 that converges on the modulation of CD44 expression and tumor plasticity. Notably, CD44 is a downstream component of the IL6/JAK/STAT3 pathway, which has been commonly associated with tumor progression, immune evasion, metastasis, and resistance to therapies [62]. Remarkably, both IFN- γ and PD-L1 signaling pathways have been reported to stimulate the activation of the IL6/JAK/STAT3 pathway in tumor contexts through various mechanisms of feedback loop, and a strong crosstalk between these pathways have been reported in literature [63–66]. Considering the increased expression of genes involved in the IL6/JAK/STAT3 pathway detected in the NSCLC-H model compared to the NSCLC-B one, we hypothesize that the concomitant activation of this signaling circuit by IFN- γ and PD-L1 might contribute to HPD development. In reference to this, the reduced activation of STAT3 in the NSCLC-H model compared to the NSCLC-B model may be due to a transient activation of this mediator, which has been documented in the literature, or to the phosphorylation of a different amino acid residue than tyrosine [67, 68]. Clearly, these hypotheses require validation through further studies, in which we will also investigate the effect of IFN- γ and PD-L1 in presence of a compromised IL6/JAK/STAT3 pathway. In parallel, further investigations will be conducted to assess the impact of NSCLC-H cells on patient-derived immune cells, either through direct interactions or secreted factors, in order to assess the CD44-mediated immunosuppressive potential.

Conclusions

In conclusion, our results suggest that immunotherapy may deeply modify cancer cell phenotype, leading to tumoral plasticity and stemness features that could be responsible for the development of HPD. Using our patient-derived cell line models, we demonstrated the existence of intrinsic tumoral responses to both the exposure of cancer cells to IFN- γ and the modulation of PD-L1 expression, which both converge to the modulation of tumoral CD44 expression, tumor plasticity and cell growth alterations. Despite our findings are strongly supported by existing literature, pointing out pro-tumor roles of both IFN- γ and PD-L1 signaling

pathways, together with the role of CD44 as a stemness marker, the mechanisms underlying this circuit are not yet fully understood and will be therefore the focus of future research. Although analyzing the mechanisms underlying HPD development based on a single patient model represents a limitation of this study, the establishment of both a baseline and a hyperprogressive cell line from the same patient provides a unique and valuable opportunity. This is particularly important given the challenges in obtaining patient-derived models that exhibit hyperprogression, a phenomenon that typically occurs at a low frequency [7]. Furthermore, the ability to compare two distinct cell lines without the need to select in vitro resistant clones offers a distinct advantage over previously published studies on HPD. Despite this limitation, our findings pave the way for understanding the intrinsic tumoral mechanisms underlying the phenomenon of HPD and for identifying novel drug targets to prevent cancer progression in patients with ICI resistance. The use of preventive strategies, including mRNA vaccines against markers overexpressed in the NSCLC-H model (e.g., CD44 isoforms, NDRG1 or ADORA1), exosome membrane-coated nanosystems, or drugs acting on epigenetic remodeling (e.g., bromodomain inhibitors) may significantly improve the clinical management of the subset of patients who develop detrimental responses to ICIs. Additionally, given the limitations of PD-L1 as a predictive biomarker for ICI therapy [33], we believe that the validation of strategies utilizing surrogate markers to assess PD-L1 and IFN- γ tumor signalosomes—such as mutations or phosphorylation status of mediators involved in canonical or alternative IFN- γ pathways—or early tumor plastic changes—for instance, the levels of CD44 expression on circulating tumor exosomes—would be essential for the selection of patients eligible for ICI therapy.

Abbreviations

NSCLC	Non-Small Cell Lung Cancer
PD-1	Programmed Cell Death Protein-1
PD-L1	Programmed Cell Death Ligand 1
ICIs	Immune Checkpoint Inhibitors
HPD	Hyperprogressive Disease
IFN- γ	Interferon-gamma
IFN- α	Interferon-alpha
IFN- β	Interferon-beta
FBS	Fetal Bovine Serum
FFPE	Formalin-fixed paraffin-embedded
H&E	Hematoxylin and Eosin
BSA	Bovine Serum Albumin
IFNGR1	Interferon-gamma receptor 1
TPS	Tumor Proportion Score
PDX	Patient-derived xenograft
TPM	Transcripts Per Kilobase Million
SNV	Single Nucleotide Variants
ECM	Extracellular Matrix
TME	Tumor Microenvironment
mAb	Monoclonal antibody

Supplementary Information

The online version contains supplementary material available at <https://doi.org/10.1186/s12967-024-06023-8>.

Additional file 1: Supplementary Materials and Methods.

Additional file 2: Table S1. List of antibodies used for Western Blot analyses. Primary antibodies by Cell Signaling Technology, except anti-actin AC-40 by Merck; secondary antibodies by Bio-Rad Laboratories.

Additional file 3: Table S2. Single nucleotide variants detected in both NSCLC-B and NSCLC-H cell lines.

Additional file 4: Table S3. CD44 gene isoform analysis. Detected isoforms, NSCLC-H vs NSCLC-B. TPM: Transcripts Per Kilobase Million.

Additional file 5: Figure S1. Transcriptomic and molecular characterization of NSCLC-B and NSCLC-H cell lines. **A** Scatter plots showing the combined projections of the first two components of a principal component analysis considering the whole transcriptome expression of NSCLC-H and NSCLC-B cells. Each cell line was analyzed in triplicate. **B i. – ii.:** top-20 GO term Biological Processes enriched in up-regulated and down-regulated genes, identified by over representation analysis of DEG; **iii. – iv.:** top-20 GO term Molecular Functions enriched in up-regulated and down-regulated genes, identified by over representation analysis of DEG. **C** GSEA enrichment plots of curated lists associated to IFN response and IL6/JAK/STAT3 pathway. **D** NDRG1 and ADORA1 transcript and protein expression. **Left:** normalized expression of *NDRG1* in NSCLC-H and NSCLC-B cells, as identified by RNAseq analysis; **middle:** western blotting picture of two distinct biological replicates and densitometric quantification of NDRG1 protein normalized on GAPDH. Expression is reported as percentage of NSCLC-H protein expression. **, $p < 0.01$ by One Sample t test. Bar represents mean with SEM; **right:** normalized expression of *ADORA1* in NSCLC-H and NSCLC-B cells, as identified by RNAseq analysis. DEG: differentially expressed genes. SEM: standard error of the mean.

Additional file 6: Figure S2. Immunostaining of NSCLC-B and NSCLC-H adherent cells. **A** CD44 and DAPI staining. White line corresponds to 20 μm . Leica widefield system, equipped with an inverted Leica DMI8 microscope, a Leica DFC9000GT CMOS camera and driven by Leica Application Suite X, working with a 40 \times dry objective. **B** PD-L1 and DAPI staining. White line corresponds to 10 μm . Leica TCS SP8 confocal microscope equipped with a Leica DMI8 inverted microscope, a tunable excitation laser source and driven by Leica Application Suite X, working with a 63 \times oil immersion objective.

Additional file 7: Figure S3. CD44 expression in patient-derived cell lines and tumor samples from ICI-resistant patients. **A** Representative histograms depicting the expression of CD44, quantified by flow-cytometry, in two NSCLC patient-derived cell lines established from biopsies of two ICI-treated patients at the moment of HPD onset, compared to CD44 expression in NSCLC-H cells. Empty histograms: unstained controls. **B** Hematoxylin and eosin staining and CD44 and PD-L1 immunohistochemical staining of tumor samples from two ICI-resistance patients, assessed in two distinct time points. **Left:** H&E; **middle:** CD44 staining; **right:** PD-L1/CD68 staining. Clinical case 1, T0: lung resection of adenocarcinoma at the time of diagnosis. CD44 staining: 37.97%, PD-L1/CD68 staining: 15%; T1: skin metastasis, CD44 staining: 62.65%, PD-L1/CD68 staining: 10%. Clinical case 2, T0: pleural effusion of adenocarcinoma at the time of diagnosis. CD44 staining: 13.10%, PD-L1/CD68 staining: 0%; T1: lymph-node metastasis, CD44 staining: 28.16%, PD-L1/CD68 staining: 0%.

Additional file 8: Figure S4. CD44 gene and CD44 transcript isoforms expression in NSCLC-B and NSCLC-H cell lines. **A** Graphical representation of the investigated CD44 transcript isoforms. Transcript isoforms in cyan were found in at least one cell line, while transcript isoforms in red were not detected. **B** Result of differential exon usage analysis using DEXSeq. The plot shows the expression of constitutive and variable exons of the CD44 gene in NSCLC-B and NSCLC-H cells. The bars below the x-axis represent exons, which are connected by lines representing the introns. The numbers at the bottom are genomic locations of CD44. The exons in pink indicate a significant differential exon usage.

Additional file 9: Figure S5. Levels of total and phosphorylated proteins involved in response to inflammatory stimuli and cell proliferation in NSCLC-B and NSCLC-H cells, in the presence or not of IFN- γ or atezolizumab treatment, as detected by Western blot analysis.

Additional file 10: Figure S6. Comparison of cell phenotype and cell behavior between NSCLC-B, NSCLC-B CL1, NSCLC-B CL2 and NSCLC-H cell lines in 2D culture conditions. **A** Expression of GFP and PD-L1 on NSCLC-B, NSCLC-B CL1, NSCLC-B CL2 and NSCLC-H cell lines, measured by cytofluorimetric analysis. Up, PD-L1 MFI: NSCLC-B, 2210; NSCLC-B CL1, 361; NSCLC-H, 501; bottom, PD-L1 MFI: NSCLC-B, 1600; NSCLC-B CL2, 990; NSCLC-H, 657. **B** Comparison of cell growth curves. Bars represent mean with SEM. Cell population doublings during 168 h of culture in 2D-growth adherent conditions were reported in the table. *, $p < 0.05$, **, $p < 0.01$ by Student's t-test. GFP: green fluorescence protein, SEM: standard error of the mean.

Acknowledgements

We thank the core facility "Centro Grandi Strumenti" (CGS) at the University of Pavia for providing access to the Confocal Microscopy and Cytofluorimetry laboratory and technical support (Dr. Patrizia Vaghi and Dr. Amanda Oldani; Dr. Samantha Solito and Dr. Alberto Azzalin).

Author contributions

AP, PLL and FG (Francesco Gelsomino) designed and coordinated the project. AP, SA, MF, MP, MDN, IS, MSS, OP, CC, SDS, FR and ICC performed the experiments. AP, SA, MF and MP collected data. AP, SA and MF analyzed the data. FR and LS conducted in vivo experiments. AP and SA drafted the manuscript with input from MR, FG (Francesco Gelsomino) and PLL. AA (Andrea Ardizzoni) and FG (Francesco Gelsomino) collected the clinical patients' data. FG (Francesca Giunchi), AA (Annalisa Altimari) and EG conducted the histological/pathological analyses. FL, MR, TC, GL and LB performed whole transcriptome sequencing analyses. PLL, FG (Francesco Gelsomino), MR, FR, CT, HDJ and LI checked the manuscript and provided valuable advice during revision stage. All authors read and approved the final manuscript.

Funding

This work was supported by Ricerca Finalizzata Ministero della Salute 2018 Grant, number GR-2018-12368031 (to Francesco Gelsomino, Francesca Giunchi and Arianna Palladini).

Availability of data and materials

All data generated or analyzed during this study are included in this published article and its supplementary information files. The RNA-sequencing datasets generated and analyzed in the current study are available to the NCBI Gene Expression Omnibus (GEO) database (<https://www.ncbi.nlm.nih.gov/geo/>) under accession number GSE255144. For revision purposes, we created a 'private access token' for distribution to journal reviewers. To create a token you'll need to log in to your 'My NCBI' account and go to: <https://www.ncbi.nlm.nih.gov/geo/query/acc.cgi?acc=GSE255144>.

Declarations

Ethics approval and consent to participate

This study was conducted in accordance with the Declaration of Helsinki (as revised in 2013). Human samples were collected after the patient gave her informed consent. The protocol was approved by the Ethics Committee Center Emilia-Romagna Region, Italy (GR-2018-12368031). Human samples and metadata including relevant clinical data were de-identified before being shared between laboratories involved in this study. All animal procedures were performed in accordance with European directive 2010/63/UE and Italian Law (No. DL26/2014). Experimental protocols were reviewed and approved by the institutional animal care and use committee of the University of Bologna and by the Italian Ministry of Health with letter 32/2020-PR.

Consent for publication

Not applicable.

Competing interests

Prof. Andrea Ardizzoni received research grants from Celgene, Bristol-Myers Squibb, Ipsen, and Roche; and honoraria for advisory roles from Bristol-Myers Squibb, Merck Sharp & Dohme, ROCHE, AstraZeneca, and Eli Lilly outside of the submitted work. Dr. Francesco Gelsomino received honoraria or personal fees for the advisory role or consulting from Eli Lilly, Novartis, AstraZeneca, Pfizer, Regeneron and Bristol-Myers Squibb outside the submitted work.

Author details

¹Medical Oncology, IRCCS Azienda Ospedaliero-Universitaria di Bologna, Bologna, Italy. ²Laboratory of Immunology and Biology of Metastasis, Department of Medical and Surgical Sciences (DIMEC), University of Bologna, Bologna, Italy. ³Pathology Unit, IRCCS Azienda Ospedaliero-Universitaria di Bologna, Bologna, Italy. ⁴Department of Molecular Medicine, University of Pavia, Pavia, Italy. ⁵Department of Biology and Biotechnology, University of Pavia, Pavia, Italy. ⁶Department of Biotechnology, University of Verona, Verona, Italy. ⁷Solid Tumor Molecular Pathology Laboratory, IRCCS Azienda Ospedaliero-Universitaria di Bologna, Bologna, Italy. ⁸Department of Medical and Surgical Sciences (DIMEC), University of Bologna, Bologna, Italy. ⁹Genartis S.R.L., Verona, Italy. ¹⁰IRCCS Azienda Ospedaliero Universitaria di Bologna, Bologna, Italy. ¹¹Unità Operativa di Oncologia, Fondazione IRCCS Policlinico San Matteo, Pavia, Italy.

Received: 3 August 2024 Accepted: 22 December 2024

Published online: 02 January 2025

References

1. Thai AA, Solomon BJ, Sequist LV, Gainor JF, Heist RS. Lung cancer. *The Lancet*. 2021;398:535–54.
2. Grant MJ, Herbst RS, Goldberg SB. Selecting the optimal immunotherapy regimen in driver-negative metastatic NSCLC. *Nat Rev Clin Oncol*. 2021;18:625–44.
3. De Giglio A, Di Federico A, Nuvola G, Deiana C, Gelsomino F. The landscape of immunotherapy in advanced NSCLC: driving beyond PD-1/PD-L1 inhibitors (CTLA-4, LAG3, IDO, OX40, TIGIT, vaccines). *Curr Oncol Rep*. 2021;23:126.
4. Shiravand Y, Khodadadi F, Kashani SMA, Hosseini-Fard SR, Hosseini S, Sadeghirad H, et al. Immune checkpoint inhibitors in cancer therapy. *Curr Oncol*. 2022;29:3044–60.
5. Puneekar SR, Shum E, Grello CM, Lau SC, Velcheti V. Immunotherapy in non-small cell lung cancer: past, present, and future directions. *Front Oncol*. 2022;12: 877594.
6. Borcoman E, Kanjanapan Y, Champiat S, Kato S, Servois V, Kurzrock R, et al. Novel patterns of response under immunotherapy. *Ann Oncol*. 2019;30:385–96.
7. Angelicola S, Ruzzi F, Landuzzi L, Scalambra L, Gelsomino F, Ardizzoni A, et al. IFN-γ and CD38 in hyperprogressive cancer development. *Cancers*. 2021;13:1–25.
8. Singavi AK, Menon S, Kilari D, Alqwasmii A, Ritch PS, Thomas JP, et al. Predictive biomarkers for hyper-progression (HP) in response to immune checkpoint inhibitors (ICI)—analysis of somatic alterations (SAs). *Ann Oncol*. 2017;28: v405.
9. Lo Russo G, Moro M, Sommariva M, Cancila V, Boeri M, Centonze G, et al. Antibody-Fc/FcR interaction on macrophages as a mechanism for hyper-progressive disease in non-small cell lung cancer subsequent to PD-1/PD-L1 blockade. *Clin Cancer Res*. 2019;25:989–99.
10. Kamada T, Togashi Y, Tay C, Ha D, Sasaki A, Nakamura Y, et al. PD-1+ regulatory T cells amplified by PD-1 blockade promote hyperprogression of cancer. *Proc Natl Acad Sci U S A*. 2019;116:9999–10008.
11. Ruzzi F, Angelicola S, Landuzzi L, Nironi E, Semprini MS, Scalambra L, et al. ADK-VR2, a cell line derived from a treatment-naïve patient with SDC4-ROS1 fusion-positive primarily crizotinib-resistant NSCLC: a novel preclinical model for new drug development of ROS1-rearranged NSCLC. *Transl Lung Cancer Res*. 2022;11:2216–29.
12. FastQC. <http://www.bioinformatics.babraham.ac.uk/projects/fastqc/>. Accessed 5 March 2024.
13. RSEM. <https://github.com/deweylab/RSEM>. Accessed 5 March 2024.

14. Yu G, Wang LG, Hu E, Luo X, Chen M, Dall'Olio G, et al. ClusterProfiler. <https://bioconductor.org/packages/release/bioc/html/clusterProfiler.html>. Accessed 5 March 2024.
15. Palladini A, Nicoletti G, Lamolinara A, Dallora M, Balboni T, Ianzano ML, et al. HER2 isoforms co-expression differently tunes mammary tumor phenotypes affecting onset, vasculature and therapeutic response. *Oncotarget*. 2017;8:54444–58.
16. De Giovanni C, Nicoletti G, Quaglino E, Landuzzi L, Palladini A, Ianzano ML, et al. Vaccines against human HER2 prevent mammary carcinoma in mice transgenic for human HER2. *Breast Cancer Res*. 2014;23(16):R10.
17. Chen C, Zhao S, Karnad A, Freeman JW. The biology and role of CD44 in cancer progression: therapeutic implications. *J Hematol Oncol*. 2018;11:64.
18. Ponta H, Sherman L, Herrlich PA. CD44: from adhesion molecules to signalling regulators. *Nat Rev Mol Cell Biol*. 2003;4:33–45.
19. Oh YM, Park HB, Shin JH, Lee JE, Park HY, Kho DH, et al. Ndrgr1 is a T-cell clonal anergy factor negatively regulated by CD28 costimulation and interleukin-2. *Nat Commun*. 2015;6:8698.
20. Liu H, Kuang X, Zhang Y, Ye Y, Li J, Liang L, et al. ADORA1 inhibition promotes tumor immune evasion by regulating the ATF3-PD-L1 axis. *Cancer Cell*. 2020;37:324–339.e8.
21. Jorgovanovic D, Song M, Wang L, Zhang Y. Roles of IFN-γ in tumor progression and regression: a review. *Biomark Res*. 2020;8:49.
22. Tang Y, Pu X, Yuan X, Pang Z, Li F, Wang X. Targeting KRASG12D mutation in non-small cell lung cancer: molecular mechanisms and therapeutic potential. *Cancer Gene Ther*. 2024;31:961–9.
23. Escors D, Gato-Cañas M, Zuazo M, Arasanz H, García-Granda MJ, Vera R, et al. The intracellular signalosome of PD-L1 in cancer cells. *Signal Transduct Target Ther*. 2018;3:26.
24. Hudson K, Cross N, Jordan-Mahy N, Leyland R. The extrinsic and intrinsic roles of PD-L1 and its receptor PD-1: implications for immunotherapy treatment. *Front Immunol*. 2020;11: 568931.
25. Yadollahi P, Jeon YK, Ng WL, Choi I. Current understanding of cancer-intrinsic PD-L1: regulation of expression and its protumoral activity. *BMB Rep*. 2021;54:12–20.
26. Alkaabi D, Arafat K, Sulaiman S, Al-Azawi AM, Attoub S. PD-1 independent role of PD-L1 in triple-negative breast cancer progression. *Int J Mol Sci*. 2023;24:6420.
27. Nieto C, Miller B, Alzofon N, Chimed T, Himes J, Joshi M, et al. The programmed death ligand 1 interactome demonstrates bidirectional signaling coordinating immune suppression and cancer progression in head and neck squamous cell carcinoma. *J Natl Cancer Inst*. 2023;115:1392–403.
28. Thapa R, Wilson GD. The importance of CD44 as a stem cell biomarker and therapeutic target in cancer. *Stem Cells Int*. 2016;2016:2087204.
29. Brabletz S, Schuhwerk H, Brabletz T, Stemmler MP. Dynamic EMT: a multi-tool for tumor progression. *EMBO J*. 2021;40: e108647.
30. Li G, Choi JE, Kryczek I, Sun Y, Liao P, Li S, et al. Intersection of immune and oncometabolic pathways drives cancer hyperprogression during immunotherapy. *Cancer Cell*. 2023;41:304–322.e7.
31. Gaitero C, Soares J, Relvas-Santos M, Peixoto A, Ferreira D, Paulo P, et al. Glycoproteogenomics characterizes the CD44 splicing code associated with bladder cancer invasion. *Theranostics*. 2022;12:3150–77.
32. Mesrati MH, Syafruddin SE, Mohtar MA, Syahir A. CD44: a multifunctional mediator of cancer progression. *Biomolecules*. 2021;11:1850.
33. Doroshov DB, Bhalla S, Beasley MB, Sholl LM, Kerr KM, Gnjatich S, et al. PD-L1 as a biomarker of response to immune-checkpoint inhibitors. *Nat Rev Clin Oncol*. 2021;18:345–62.
34. Tamai K, Nakamura M, Mizuma M, Mochizuki M, Yokoyama M, Endo H, et al. Suppressive expression of CD274 increases tumorigenesis and cancer stem cell phenotypes in cholangiocarcinoma. *Cancer Sci*. 2014;105:667–74.
35. Wang X, Yang X, Zhang C, Wang Y, Cheng T, Duan L, et al. Tumor cell-intrinsic PD-1 receptor is a tumor suppressor and mediates resistance to PD-1 blockade therapy. *PNAS*. 2020;117:6640–50.
36. Yu W, Hua Y, Qiu H, Hao J, Zou K, Li Z, et al. PD-L1 promotes tumor growth and progression by activating WIP and β-catenin signaling pathways and predicts poor prognosis in lung cancer. *Cell Death Dis*. 2020;11:506.
37. Gao L, Guo Q, Li X, Yang X, Ni H, Wang T, et al. MiR-873/PD-L1 axis regulates the stemness of breast cancer cells. *EBioMedicine*. 2019;41:395–407.

38. Mansour FA, Al-Mazrou A, Al-Mohanna F, Al-Alwan M, Ghebeh H. PD-L1 is overexpressed on breast cancer stem cells through notch3/mTOR axis. *Oncoimmunology*. 2020;9:1729299.
39. Hong W, Xue M, Jiang J, Zhang Y, Gao X. Circular RNA circ-CPA4/let-7 miRNA/PD-L1 axis regulates cell growth, stemness, drug resistance and immune evasion in non-small cell lung cancer (NSCLC). *J Exp Clin Cancer Res*. 2020;39:149.
40. Kong T, Ahn R, Yang K, Zhu X, Fu Z, Morin G, et al. CD44 promotes PD-L1 expression and its tumor-intrinsic function in breast and lung cancers. *Cancer Res*. 2020;80:444–57.
41. Zhang C, Wang H, Wang X, Zhao C, Wang H. CD44, a marker of cancer stem cells, is positively correlated with PD-L1 expression and immune cells infiltration in lung adenocarcinoma. *Cancer Cell Int*. 2020;20:583.
42. Subhadarshini S, Sahoo S, Debnath S, Somarelli JA, Kumar Jolly M. Dynamical modelling of proliferative-invasive plasticity and IFN γ signaling in melanoma reveals mechanisms of PD-L1 expression heterogeneity. *bioRxiv*. 2023; <https://doi.org/10.1101/2023.01.09.523355>.
43. Cao H, Xiang Y, Zhang S, Chao Y, Guo J, Aurich T, et al. PD-L1 regulates inflammatory programs of macrophages from human pluripotent stem cells. *Life Sci Alliance*. 2024;7: e202302461.
44. Mimura K, Teh JL, Okayama H, Shiraiishi K, Kua LF, Koh V, et al. PD-L1 expression is mainly regulated by interferon gamma associated with JAK-STAT pathway in gastric cancer. *Cancer Sci*. 2018;109:43–53.
45. Han T, Wang X, Shi S, Zhang W, Wang J, Wu Q, et al. Cancer cell resistance to IFN γ can occur via enhanced double-strand break repair pathway activity. *Cancer Immunol Res*. 2023;11:381–98.
46. Kalbasi A, Ribas A. Tumour-intrinsic resistance to immune checkpoint blockade. *Nat Rev Immunol*. 2020;20:25–39.
47. Platanias LC. Mechanisms of type-I- and type-II-interferon-mediated signalling. *Nat Rev Immunol*. 2005;5:375–86.
48. Barrat FJ, Crow MK, Ivashkiv LB. Interferon target-gene expression and epigenomic signatures in health and disease. *Nat Immunol*. 2019;20:1574–83.
49. Benci JL, Xu B, Qiu Y, Wu TJ, Dada H, Twyman-Saint Victor C, et al. Tumor interferon signaling regulates a multigenic resistance program to immune checkpoint blockade. *Cell*. 2016;167:1540–1554.e12.
50. Memon D, Schoenfeld AJ, Ye D, Fromm G, Rizvi H, Zhang X, et al. Clinical and molecular features of acquired resistance to immunotherapy in non-small cell lung cancer. *Cancer Cell*. 2024;42:209–224.e9.
51. Majoros A, Platanitis E, Kernbauer-Hözl E, Rosebrock F, Müller M, Decker T. Canonical and non-canonical aspects of JAK–STAT signaling: lessons from interferons for cytokine responses. *Front Immunol*. 2017;8.
52. Ivashkiv LB. IFN γ : signalling, epigenetics and roles in immunity, metabolism, disease and cancer immunotherapy. *Nat Rev Immunol*. 2018;18:545–58.
53. Kearney SJ, Delgado C, Eshleman EM, Hill KK, O'Connor BP, Lenz LL. Type I IFNs downregulate myeloid cell IFN- γ receptor by inducing recruitment of an early growth response 3/NGF1-A binding protein 1 complex that silences ifngr1 transcription. *J Immunol*. 2013;191:3384–92.
54. Crisler WJ, Eshleman EM, Lenz LL. Ligand-induced IFNGR1 down-regulation calibrates myeloid cell IFN γ responsiveness. *Life Sci Alliance*. 2019;2: e201900447.
55. Robbins EW, Travanty EA, Yang K, Iczkowski KA. MAP kinase pathways and calcitonin influence CD44 alternate isoform expression in prostate cancer cells. *BMC Cancer*. 2008;8:260.
56. Ng CT, Fong LY, Sulaiman MR, Moklas MAM, Yong YK, Hakim MN, et al. Interferon-gamma increases endothelial permeability by causing activation of p38 MAP kinase and actin cytoskeleton alteration. *J Interferon Cytokine Res*. 2015;35:513–22.
57. Vella V, De Francesco EM, Bonavita E, Lappano R, Belfiore A. IFN-I signaling in cancer: the connection with dysregulated Insulin/IGF axis. *Trends Endocrinol Metab*. 2022;33:569–86.
58. Hiltbrunner S, Cords L, Kasser S, Freiberger SN, Kreutzer S, Toussaint NC, et al. Acquired resistance to anti-PD1 therapy in patients with NSCLC associates with immunosuppressive T cell phenotype. *Nat Commun*. 2023;14:5154.
59. Song M, Ping Y, Zhang K, Yang L, Li F, Zhang C, et al. Low-dose IFN γ induces tumor cell stemness in tumor microenvironment of non-small cell lung cancer. *Cancer Res*. 2019;79:3737–48.
60. Beziaud L, Young CM, Alonso AM, Norkin M, Minafra AR, Huelsken J. IFN γ -induced stem-like state of cancer cells as a driver of metastatic progression following immunotherapy. *Cell Stem Cell*. 2023;30:818–831.e6.
61. Pérez-González A, Bévart K, Blanpain C. Cancer cell plasticity during tumor progression, metastasis and response to therapy. *Nat Cancer*. 2023;4:1063–82.
62. Huang B, Lang X, Li X. The role of IL-6/JAK2/STAT3 signaling pathway in cancers. *Front Oncol*. 2022;12.
63. Qi Y, Huang Y, Wang H, Zhang Y, Bao Y, Sun L, et al. Elucidating the crosstalk mechanism between IFN- γ and IL-6 via mathematical modelling. *BMC Bioinformatics*. 2013;14:41.
64. Song TL, Nairismägi ML, Laurensia Y, Lim JQ, Tan J, Li ZM, et al. Oncogenic activation of the STAT3 pathway drives PD-L1 expression in natural killer/T-cell lymphoma. *Blood*. 2018;132:1146–58.
65. Zhang W, Liu Y, Yan Z, Yang H, Sun W, Yao Y, et al. IL-6 promotes PD-L1 expression in monocytes and macrophages by decreasing protein tyrosine phosphatase receptor type O expression in human hepatocellular carcinoma. *J Immunother Cancer*. 2020;8: e000285.
66. Chuangchot N, Jamjuntra P, Yangngam S, Luangwattananun P, Thongchot S, Junking M, et al. Enhancement of PD-L1-attenuated CAR-T cell function through breast cancer-associated fibroblasts-derived IL-6 signaling via STAT3/AKT pathways. *Breast Cancer Res*. 2023;25:86.
67. Johnson DE, O'Keefe RA, Grandis JR. Targeting the IL-6/JAK/STAT3 signaling axis in cancer. *Nat Rev Clin Oncol*. 2018;15:234–48.
68. Arévalo J, Campoy I, Durán M, Nemours S, Areny A, Vall-Palomar M, et al. STAT3 phosphorylation at serine 727 activates specific genetic programs and promotes clear cell renal cell carcinoma (ccRCC) aggressiveness. *Sci Rep*. 2023;13:19552.

Publisher's Note

Springer Nature remains neutral with regard to jurisdictional claims in published maps and institutional affiliations.